

Proteomic and Functional Analyses Reveal a Mitochondrial Dysfunction in P301L Tau Transgenic Mice*

Received for publication, January 11, 2005, and in revised form, April 13, 2005
Published, JBC Papers in Press, April 14, 2005, DOI 10.1074/jbc.M500356200

Della C. David[‡], Susanne Hauptmann^{§¶}, Isabel Scherping^{§¶}, Katrin Schuessel[§], Uta Keil[§],
Patrizia Rizzu^{||}, Rivka Ravid^{**}, Stefan Dröse^{‡‡}, Ulrich Brandt^{‡‡}, Walter E. Müller[§],
Anne Eckert^{§§}, and Jürgen Götz^{‡¶¶}

From the [‡]Division of Psychiatry Research, University of Zurich, 8008 Zurich, Switzerland, and [§]Department of Pharmacology, Biocentre, University of Frankfurt, 60439 Frankfurt, Germany, ^{||}Department of Human Genetics, Section of Medical Genomics and Center for Neurogenomics and Cognitive Research, VU University Medical Center and VU University, 1081 BT Amsterdam, The Netherlands, ^{**}The Netherlands Brain Bank, 1105 AZ Amsterdam, The Netherlands, ^{‡‡}Center for Biological Chemistry, University of Frankfurt, 60590 Frankfurt, Germany, and ^{§§}Neurobiology Research Laboratory, Psychiatric University Clinic, 4025 Basel, Switzerland

Transgenic mice overexpressing the P301L mutant human tau protein exhibit an accumulation of hyperphosphorylated tau and develop neurofibrillary tangles. The consequences of tau pathology were investigated here by proteomics followed by functional analysis. Mainly metabolism-related proteins including mitochondrial respiratory chain complex components, antioxidant enzymes, and synaptic proteins were identified as modified in the proteome pattern of P301L tau mice. Significantly, the reduction in mitochondrial complex V levels in the P301L tau mice revealed using proteomics was also confirmed as decreased in human P301L FTDP-17 (frontotemporal dementia with parkinsonism linked to chromosome 17) brains. Functional analysis demonstrated a mitochondrial dysfunction in P301L tau mice together with reduced NADH-ubiquinone oxidoreductase activity and, with age, impaired mitochondrial respiration and ATP synthesis. Mitochondrial dysfunction was associated with higher levels of reactive oxygen species in aged transgenic mice. Increased tau pathology as in aged homozygous P301L tau mice revealed modified lipid peroxidation levels and the up-regulation of antioxidant enzymes in response to oxidative stress. Furthermore, P301L tau mitochondria displayed increased vulnerability toward β -amyloid ($A\beta$) peptide insult, suggesting a synergistic action of tau and $A\beta$ pathology on the mitochondria. Taken together, we conclude that tau pathology involves a mitochondrial and oxidative stress disorder possibly distinct from that caused by $A\beta$.

β -amyloid ($A\beta$) peptides and intracellular neurofibrillary tangles (NFTs) composed of hyperphosphorylated tau protein (1, 2). Mutations in tau have been identified in a related neurodegenerative disorder called frontotemporal dementia with parkinsonism linked to chromosome 17 (FTDP-17) with NFT formation in the absence of plaque formation (3–5). Transgenic mice overexpressing the P301L mutant human tau protein were created to model tauopathies *in vivo* (6, 7). These mice show an accumulation of hyperphosphorylated tau and NFT formation similar to those in FTDP-17 and AD.

Little is known about the distinct intracellular mechanisms underlying the consequences of tau pathology. This insight could help us to understand the selective vulnerability of cells with tau pathology and thereby the pathogenesis of AD. Increasing evidence highlights a connection between AD and mitochondrial dysfunction together with a deregulation of energy metabolism and oxidative stress (8). Various reports have demonstrated markedly reduced levels of mitochondrial proteins and activities (9–11), decreased glucose turnover (12, 13), increased mitochondrial DNA mutations (14–16), and increased lipid peroxidation (17–19) in AD brains.

To examine the contribution of tau to these neurodegenerative processes, we carried out a proteomic analysis of our P301L tau transgenic mice. To zoom in on proteins relevant to the pathology, we sequentially extracted whole brains from six pairs of P301L tau and wild-type (WT) mice into three fractions according to protein solubility. Comparative analysis of two-dimensional gels run for each fraction revealed statistically significant differences between P301L tau and WT mice. We found three principal categories of proteins differentially regulated by P301L tau expression: metabolism-related proteins including mitochondrial respiratory chain complex components, oxidative stress-related enzymes implicated in reactive oxygen species (ROS) detoxification, and synapse-related pro-

Alzheimer disease (AD)¹ is characterized by two major histopathological hallmarks, extracellular plaques of fibrillar

* This work was supported by grants from the EMDO Foundation, the Olga Mayenfisch Foundation, the Kurt und Senta Herrmann Foundation, the National Centers of Competence in Research on Neural Plasticity and Repair, and the Swiss National Science Foundation (to J. G.); Swiss National Science Foundation (to A. E.); Deutsche Forschungsgemeinschaft Grant SFB 472-P2 (to U. B.); and a grant from Hirnliga e.V. (to U. K.). The costs of publication of this article were defrayed in part by the payment of page charges. This article must therefore be hereby marked "advertisement" in accordance with 18 U.S.C. Section 1734 solely to indicate this fact.

^{¶¶} Both authors contributed equally to this work.

^{¶¶¶} To whom correspondence should be addressed: Brain and Mind Research Institute, University of Sydney, 100 Mallet St., Camperdown, NSW 2050, Australia. Tel.: 61-2-9351-0799; Fax: 61-2-9351-0652; E-mail: jgoetz@med.usyd.edu.au.

¹ The abbreviations used are: AD, Alzheimer disease; FTDP-17, fron-

totemporal dementia with parkinsonism linked to chromosome 17; NFT, neurofibrillary tangle; $A\beta$, β -amyloid; WT, wild-type; ROS, reactive oxygen species; GST, glutathione S-transferase; SOD, superoxide dismutase; GR, glutathione reductase; DRP, dihydropyrimidinase-related protein; MALDI, matrix-assisted laser desorption ionization; TOF/TOF, tandem time-of-flight; MDA, malondialdehyde; DBQ, *n*-deacylubi-quinone; FCCP, carbonyl cyanide *p*-trifluoromethoxyphenylhydrazone; HAR, hexaammineruthenium(III)-chloride; CHAPS, 3-[(3-cholamidopropyl)dimethylammonio]-1-propanesulfonic acid; DHE, dihydroethidium; H₂DCF-DA, 2',7'-dichlorodihydrofluorescein diacetate; PIPES, 1,4-piperazinediethanesulfonic acid; MOPS, 4-morpholinepropanesulfonic acid; ANOVA, analysis of variance; IPG, immobilized pH gradient.

teins. Consistent with these findings, P301L tau mice exhibited mitochondrial functional defects together with reduced electron transport chain complex I activity. Aged P301L tau mice showed impaired mitochondrial respiration, reduced complex V activity, and higher levels of ROS than WT controls. Furthermore, modified lipid peroxidation and increased antioxidant enzyme activities were detected in aged homozygous mice. We also found an increased vulnerability of P301L tau mitochondria to A β insult, suggesting a synergistic action of tau and A β pathology on the mitochondria. Corroborating the P301L tau mouse mitochondrial deficits, we could demonstrate a reduction in complex V levels in human P301L FTDP-17 brains, implying a potential mitochondrial dysfunction in human patients afflicted with this neurodegenerative disorder.

EXPERIMENTAL PROCEDURES

Transgenic Mice—The transgenic mice used in the present study express the human pathogenic mutation P301L of tau together with the longest human brain tau isoform (htau40) under control of the neuron-specific mThy1.2 promoter (7). This isoform contains exons 2 and 3 as well as four microtubule-binding repeats (2⁺3⁺4R, human tau40). Pronuclear injections were done into C57Bl/6 \times DBA/2 F₂ oocytes to obtain founder animals that were back-crossed with C57Bl/6 mice to establish transgenic lines. In addition, homozygous P301L tau mice were obtained and confirmed by TaqMan real-time quantitative PCR (data not shown).

Different age sets of mice were used for different experimental procedures corresponding to various stages in the development of tau pathology. P301L tau mice show tau hyperphosphorylation already at 3 months (7). NFT formation starts at 6 months of age (20). We used 8.5–10-month-old mice for the proteomics analysis to study the consequences of tau pathology at the beginning of NFT formation without the influence of aging. At a similar age (*i.e.* 12 months old), mitochondrial membrane potential and complex I and IV activity were determined. ATP levels, mitochondrial respiration, and ROS levels were analyzed in mice at 12 and 24 months of age. 24-month-old mice are expected to bear the highest levels of tau pathology. 18-month-old mice were used to determine mitochondrial numbers in neurites. This intermediate age allows us to see the full effect of tau pathology on mitochondrial transport without pronounced aging effects such as those seen in 24-month-old mice. Finally, 12- and 24-month-old homozygous, hemizygous, and wild-type mice were tested for lipid peroxidation.

Sequential Extraction of Brain Samples—Four pairs of 8.5-month-old male hemizygous P301L tau and WT control mice and two pairs of 10-month-old male hemizygous P301L tau and WT control mice were sacrificed by cervical dislocation, and brains were removed at 4 °C and snap-frozen in liquid nitrogen. Brains were sequentially extracted with the ReadyPrep sequential extraction kit (Bio-Rad) according to a modified version of the manufacturer's protocol. Only one P301L tau and one WT each were extracted at a time. All steps were carried out at 4 °C, unless otherwise specified. Briefly, whole brains were homogenized in 3 ml of buffer 1 (40 mM Tris, pH 7.4, Complete protease inhibitor mixture (Roche Diagnostics), 0.5 mg/ml Pefabloc (Roche Applied Science), 1 mM Na₂V₀₄, and 1 mM NaF) and 200 units of DNase I in a glass-Teflon potter. After 15 min on ice, the homogenate was centrifuged at 15,000 \times *g* for 15 min. Supernatant E1 was collected for further analysis. The pellet was washed twice with buffer 1 before it was resuspended in 750 μ l of buffer 2 (8 M urea, 4% CHAPS, 40 mM Tris, 0.2% Bio-Lyte 3/10 ampholytes (Bio-Rad), and 2 mM tributylphosphine), incubated for 10 min at room temperature, and ultra-centrifuged at 57,000 \times *g* for 30 min. Supernatant E2 was collected for further analysis. The pellet was washed once with buffer 2 and then resuspended in buffer 3 (5 M urea, 2 M thiourea, 2% CHAPS, 2% caprylyl sulfoetabine 3–10, 40 mM Tris, 0.2% Bio-Lyte 3/10 ampholytes, and 2 mM tributylphosphine). The final supernatant, E3, was collected after ultra-centrifugation at 89,000 \times *g* for 30 min at 10 °C.

Two-dimensional Gel Electrophoresis—Isoelectrical focusing was carried out using the PROTEAN IEF Cell (Bio-Rad). Six P301L tau transgenic and six WT samples were focused simultaneously. Each fraction from the sequential extraction (40 μ g of E1, 50 μ g of E2, or 60 μ l of E3) was loaded on 17-cm IPG strips (pH 3–10; Bio-Rad) in rehydration buffer (8.5 M urea, 4% CHAPS, 0.5% pharmalytes (pH 3–10; Amersham Biosciences), and 1.2% DeStreak reagent (Amersham Biosciences)). After passive rehydration for 15 h, the IPG strips were isoelectrically focused following a stepwise increase in voltage from 150 to

10,000 V, finishing with 60,000 V-h. Prior to SDS-PAGE, the IPG strips were equilibrated in 2% dithiothreitol, 6 M urea, 2% SDS, 0.05 M Tris, pH 8.8, and 20% glycerol for 30 min and then equilibrated again in the same buffer with 2.5% iodoacetamide instead of dithiothreitol for another 30 min. Second dimension separation was performed on 12% SDS-polyacrylamide gels at 200 V using the PROTEAN Plus Dodeca cell electrophoresis system (Bio-Rad). All gels of the six P301L tau transgenic and six WT samples from one fraction were run at the same time.

Gel Staining and Image Analysis—Gels were stained using a modified silver staining method (21). Six P301L tau transgenic and six WT two-dimensional gels were compared simultaneously with the Proteomweaver imaging software Version 2.1 (Definiens, Munich, Germany). This software normalizes all gels and compares each two-dimensional spot pattern of every transgenic gel of one fraction with each two-dimensional spot pattern of every WT gel of the same fraction. Only spots present in all 12 gels and differentially regulated by at least 1.5-fold were considered for statistical analysis with Student's *t* test (*p* < 0.05).

Mass Spectrometry—For mass spectrometry analysis, 150 μ g of E1, 150 μ g of E2, and 180 μ l of E3, respectively, were loaded on 24-cm IPG strips (pH 3–10). The two-dimensional gels were stained with Sypro Ruby (Molecular Probes, Invitrogen), and the protein spots of interest were excised with the GelPix protein spot excision system (Genetix, Hampshire, UK). Spots were prepared for in-gel trypsin digestion. Briefly, spots were washed twice with double-distilled H₂O, once with 50 mM NH₄HCO₃/30% acetonitrile for 5 min at 37 °C, and once with 80% acetonitrile for 10 min at room temperature. Digestion was carried out with 30 ng trypsin/spot in 10 mM Tris, pH 8.3, 2 mM CaCl₂ for 3 h at 37 °C. After 5 min of sonication, the tryptic digests were desalted and concentrated using μ -C18 ZipTips (Millipore, Volketswil, Switzerland). The bound peptides were eluted directly onto the MALDI target with 0.8 μ l of α -cyano-4-hydroxycinnamic acid matrix (5 mg/ml) in 65% acetonitrile, 35% double-distilled H₂O containing 0.1% trifluoroacetic acid. Digests were analyzed by MALDI tandem time-of-flight (TOF/TOF) mass spectrometry using a 4700 Proteomics Analyzer MALDI-TOF/TOF mass spectrometer (Applied Biosystems). One mass spectrum and up to five tandem mass spectra of all precursor ions with a minimum signal/noise ratio of 80 were recorded for each sample spot. Autoproteolytic fragments of trypsin were used as internal calibrants in the mass spectrometry mode. The mass and tandem mass spectra were analyzed using Mascot (Matrix Science, London, UK; available at www.matrixscience.com) as the search engine. A combined mass spectrometry and tandem mass spectrometry search with a peptide tolerance of 25 ppm and a tandem mass spectrometry tolerance of 0.2 Da was carried out against the UniProt complete mouse proteome data base (available at ftp://ftp.ebi.ac.uk/pub/databases/integr8). Protein identification was considered significant if the Mascot score was higher than the probability *p* < 0.05 of a random match.

Evaluation of Complex V Level in Human Brains—Homogenates from temporal cortex of two controls and four P301L FTDP-17 patients were prepared in 150 mM Tris, pH 6.8, 2.5% SDS, 8 M urea, 20% glycerol, 10% β -mercaptoethanol, and 0.1% bromophenol blue and subjected to Western blotting using standard methods. 2.5 μ l of total brain lysate were loaded. The blots were developed with antibodies directed against the complex V component ATP synthase chain D (A21343, 0.2 μ g/ml; Molecular Probes) and against porin for normalization (A31855, 0.2 μ g/ml; Molecular Probes). As a secondary antibody, a goat anti-mouse IgG (Amersham Biosciences, 1:5000) was used. Non-overexposed films were used to quantify the bands with Image J software (National Institutes of Health; available at rsb.info.nih.gov/ij/). Complex V levels were expressed as a percentage of porin levels.

Samples used (as loaded) were as follows: 1) control brain, 73-year-old female; 2) control brain, 72-year-old male; 3) P301L brain, 64-year-old female; 4) P301L brain, 52-year-old male; 5) P301L brain, 66-year-old female; and 6) P301L brain, 60-year-old male. Three other control samples were used (specifically, control temporal cortex from 78-year-old female, 82-year-old female, and 78-year-old male brains) (data not shown).

Materials Used for Mitochondrial Analysis—Rhodamine 123, tetramethylrhodamine-ethyl ester, and MitoTracker Green FM were purchased from Molecular Probes Europe (Leiden, The Netherlands); 2',7'-dichlorodihydrofluorescein diacetate (H₂DCF-DA) and dihydroethidium (DHE) were purchased from Calbiochem (Merck Biosciences, Bad Soden, Germany); hydrochloric acid, ethanol, ferric chloride, and chloroform were purchased from VWR International (Darmstadt, Germany); and the ViaLight HT kit was purchased from Cambrex Bio Science (Copenhagen, Denmark). The Cytochrome *c* Oxidase (Complex IV) As-

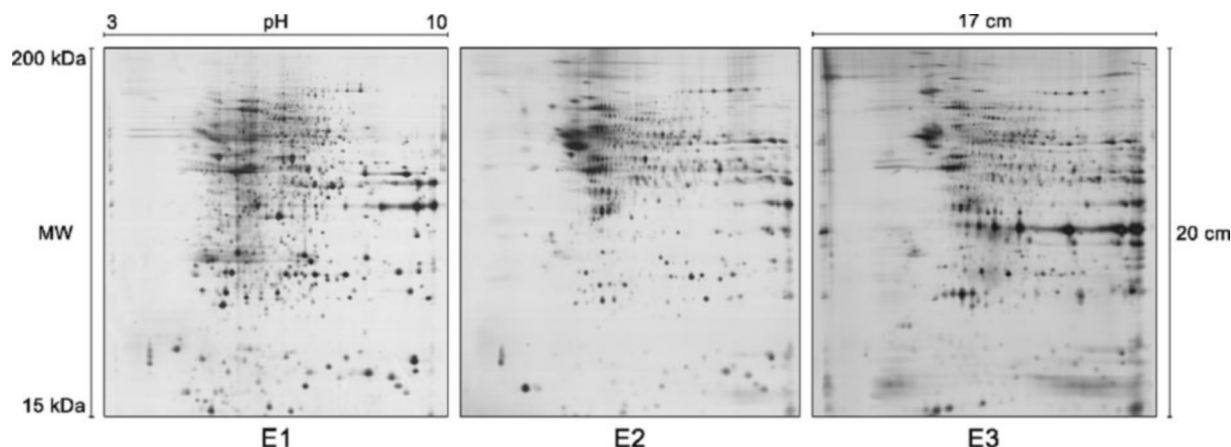


FIG. 1. **Representative two-dimensional gels.** Six P301L tau and six WT brains were sequentially extracted. Fractions E1 (soluble proteins), E2 (intermediate soluble), and E3 (less soluble) were separated by two-dimensional gel electrophoresis. Differential spot expression was evaluated with Proteomweaver, and significantly regulated spots found between transgenic and wild-type two-dimensional gels were identified by mass spectrometry. Representative gels of each fraction are shown.

say Kit, sodium nitroprusside, rotenone, thenoyltrifluoroacetone, antimycin, sodium azide (NaN_3), and oligomycin were obtained from Sigma-Aldrich. $\text{A}\beta_{1-42}$ (Bachem, Weil am Rhein, Germany) was dissolved in Tris-buffered saline, pH 7.4, at a concentration of 1 mM and stored at -20°C . The stock solution was diluted in Tris-buffered saline to the desired concentrations and incubated at 37°C for 24 h to obtain aged, aggregated preparations of $\text{A}\beta_{1-42}$. All aqueous solutions were prepared with deionized and filtered water (Millipore).

Brain Tissue Preparation for Mitochondrial Analysis—Mice (8 pairs of 12-month-old and 8 pairs of 24-month-old hemizygous P301L tau and WT control mice) were sacrificed by decapitation, and brains were quickly dissected on ice (described in Ref. 22, with modification). After removing the cerebellum, one hemisphere (the other hemisphere was directly used for preparation of isolated mitochondria) was minced into 1 ml of medium I (138 mM NaCl, 5.4 mM KCl, 0.17 mM Na_2HPO_4 , 0.22 mM K_2PO_4 , 5.5 mM glucose, and 58.4 mM sucrose, pH 7.35) with a scalpel and further dissociated by trituration through a nylon mesh (pore diameter, 1 mm) with a Pasteur pipette. The resulting suspension was filtered by gravity through a fresh nylon mesh with a pore diameter of 102 μm , and the dissociated cell aggregates were washed twice with medium II (110 mM NaCl, 5.3 mM KCl, 1.8 mM $\text{CaCl}_2\cdot\text{H}_2\text{O}$, 1 mM $\text{MgCl}_2\cdot 6\text{H}_2\text{O}$, 25 mM glucose, 70 mM sucrose, 20 mM HEPES, pH 7.4) by centrifugation ($400 \times g$ for 3 min at 4°C). 100 μl of the suspension were used for protein determination. After centrifugation, cells were resuspended in 3 ml of Dulbecco's modified Eagle's medium, and then aliquots (100 μl /well) were distributed in a white 96-well plate for measurement of ATP levels, and aliquots (250 μl /well) were distributed in a 48-well plate for measurement of the mitochondrial membrane potential and ROS levels. The latter were maintained at 37°C in a humidified atmosphere of 5% CO_2 /95% air for the staining period with the appropriate dye or incubated with $\text{A}\beta$ for 4 h. The preparations of cortical cells from P301L tau transgenic mice and WT littermate controls (crossover design) were made within 2 h under the same conditions and in parallel. Data are expressed as fluorescence units per mg/ml protein. The total protein content was determined (23).

Determination of the Mitochondrial Membrane Potential ψ_m —The membrane potential of the inner mitochondrial membrane was measured using Rhodamine 123 dye added to the cell culture medium at a final concentration of 0.4 μM for 15 min. Cells were washed twice with Hank's balanced salt solution (Sigma), and fluorescence was determined with a Victor2 multiplate reader (PerkinElmer Life Sciences) at 490 nm (excitation)/535 nm (emission). Loading capacity of the dye within the membrane decreases when the mitochondrial membrane potential declines after damage, e.g. exposure to $\text{A}\beta_{1-42}$. For the secondary insult with $\text{A}\beta_{1-42}$, cells were incubated for 4 h with 50 nM pre-aggregated $\text{A}\beta_{1-42}$.

To test acute and fast changes in ψ_m , the fluorescent dye tetramethylrhodamine-ethyl ester was used at 0.4 μM for 15 min. Tetramethylrhodamine-ethyl ester exhibits a characteristic increase in fluorescence at 490 nm (excitation)/590 nm (emission) after challenging mitochondria with drugs that decrease the membrane potential. The mitochondrial membrane potential was recorded with the respiratory inhibitors rotenone (2 μM), thenoyltrifluoroacetone (10 μM), antimycin (2 μM), oligomycin (10 μM), and sodium azide (10 mM) (24, 25).

ATP Levels—ATP levels were determined with a bioluminescence assay (ViaLight HT; Cambrex Bio Science). The enzyme luciferase, which catalyzes the formation of light from ATP and luciferin, was utilized. The emitted light was linearly related to the ATP concentration and measured using a luminometer (26).

ROS Levels—Levels of cytosolic ROS were measured using the fluorescent probe $\text{H}_2\text{DCF-DA}$, and levels of superoxide anion radical were measured by using DHE. Brain cells were loaded for 15 min with 10 μM $\text{H}_2\text{DCF-DA}$ or 10 μM DHE. After washing twice with Hank's balanced salt solution, formation of the fluorescent product dichlorofluorescein was detected with Victor2 multiplate reader (PerkinElmer Life Sciences) at 485 nm (excitation)/535 nm (emission). Dichlorofluorescein is trapped mainly in the cytoplasm and oxidized by several ROS, most notably hydrogen peroxide (27). DHE, which is oxidized to the fluorescent ethidium cation by O_2^- was detected with Victor2 multiplate reader at 490 nm (excitation)/590 nm (emission) (28).

Amount of Mitochondria—The total amount of mitochondria was measured using the cell-permeable mitochondrion-selective dye Mito-Tracker Green FM (100 nM, 15 min) which is essentially nonfluorescent in aqueous solutions and only becomes fluorescent once it accumulates in the lipid environment of mitochondria (490 nm, excitation; 516 nm, emission). To determine the number of mitochondria, in addition, four pairs of 18-month-old P301L tau transgenic and WT mice were perfused transcardially with 4% paraformaldehyde in microtubule stabilization buffer (65 mM PIPES, 25 mM HEPES, 10 mM EGTA, and 3 mM MgCl_2 , pH 6.9). 5- μm paraffin brain sections were co-immunostained with anti-porin (A31855, diluted 1:2000; Molecular Probes) and anti-tubulin (YOL 1/34, 1:600; Abcam Limited, Cambridge, UK) antibodies, followed by incubation with Cy3- and Cy2-conjugated secondary antibodies (Jackson ImmunoResearch, Milan Analytic, Fribourg, Switzerland). The number of mitochondria in neurites of CA1 hippocampal neurons was counted both proximal and distal to the cell body.

Preparation of Isolated Mitochondria—Mice were sacrificed by decapitation, and one brain hemisphere was rapidly dissected on ice and washed in an ice-cold buffer (210 mM mannitol, 70 mM sucrose, 10 mM HEPES, 1 mM EDTA, 0.45% bovine serum albumin, 0.5 mM dithiothreitol, and Complete protease inhibitor mixture tablets (Roche Diagnostics)). After removing the cerebellum, the tissue sample was homogenized in 2 ml of buffer with a glass homogenizer (10–15 strokes, 400 rpm), and the resulting homogenate was centrifuged at $1400 \times g$ for 7 min at 4°C to remove nuclei and tissue particles. The low-speed centrifugation step was repeated once with the supernatant. Then, the supernatant fraction was centrifuged at $10,000 \times g$ for 5 min at 4°C to pellet mitochondria. The resulting pellet was resuspended in 1 ml of ice-cold buffer and centrifuged again at $800 \times g$ for 3 min at 4°C . Finally, the mitochondria-enriched supernatant was centrifuged at $10,000 \times g$ for 5 min at 4°C to obtain a mitochondrial fraction. This fraction was resuspended in 100 μl of ice-cold buffer and stored at 4°C until use, followed by determination of protein content (23).

Mitochondrial Respiration—The rate of mitochondrial respiration was monitored at 25°C using an Oxygraph-2k system (Oroboros, Innsbruck, Austria) equipped with two chambers and DatLab software. Mitochondria (0.5 mg) were added to 2 ml of a buffer containing 65 mM sucrose, 10 mM potassium phosphate, 10 mM Tris-HCl, 10 mM MgSO_4 ,

TABLE I
Protein alterations in P301L tau mice

| Protein | Accession no. ^a | Fraction ^b | Spot no. | Fold difference | Student's <i>t</i> test | Mascot score ^c |
|---|----------------------------|-----------------------|----------|-----------------|-------------------------|---------------------------|
| Proteins involved in mitochondrial respiration and metabolism | | | | | | |
| NADH-ubiquinone oxidoreductase 30-kDa subunit | Q9DCT2 | E2 | 375 | -1.62 | 0.0089 | 101 |
| ATP synthase D chain | Q9DCX2 | E2 | 455 | -1.90 | 0.0124 | 134 |
| ATP synthase D chain | Q9DCX2 | E2 | 1457 | -1.66 | 0.0026 | 62 |
| Triosephosphate isomerase | P17751 | E2 | 750 | -1.79 | 0.0139 | 71 |
| Inorganic pyrophosphatase (2010317E03Rik protein) | Q9D819 | E1 | 576 | 1.56 | 0.0007 | 218 |
| Malate dehydrogenase, cytoplasmic | P14152 | E1 | 323 | -1.58 | 0.0096 | 63 |
| Proteins involved in oxidative stress | | | | | | |
| Peroxisome oxidoreductin 6 | O08709 | E2 | 38 | -1.90 | 0.0076 | 287 |
| Thioredoxin-dependent peroxide reductase (perioxisome oxidoreductin 3) | P20108 | E2 | 978 | -1.76 | 0.0007 | 91 |
| GSTP2 | P19157 | E2 | 443 | -1.68 | 0.0104 | 158 |
| GSTMu 1 | P10649 | E2 | 622 | -1.61 | 0.0145 | 182 |
| Phospholipid hydroperoxide glutathione peroxidase | O70325 | E1 | 1605 | -1.57 | 0.0168 | 98 |
| Synapse-related proteins | | | | | | |
| DRP-2 | O08553 | E1 | 311 | 1.50 | 0.0074 | 305 |
| DRP-2 | O08553 | E1 | 1983 | 1.53 | 0.0136 | 103 |
| DRP-2 | O08553 | E2 | 1853 | 1.62 | 0.0001 | 222 |
| DRP-2 | O08553 | E2 | 140 | 1.59 | 0.0000 | 133 |
| DRP-2 | O08553 | E2 | 1289 | 1.51 | 0.0001 | 105 |
| DRP-3 | Q62188 | E1 | 1307 | 1.64 | 0.0217 | 81 |
| Synapsin I | O88935 | E2 | 1597 | 1.91 | 0.0069 | 172 |
| Synapsin I | O88935 | E2 | 2160 | 1.83 | 0.0077 | 140 |
| Septin 11 | Q8C1B7 | E2 | 1589 | 1.70 | 0.0152 | 122 |
| Septin 5 (CDCrel-1) | Q9Z2Q6 | E2 | 2112 | 1.59 | 0.0002 | 341 |
| Other proteins | | | | | | |
| Stathmin ^d | P54227 | E1 | 2156 | -1.66 | 0.0081 | 55 ^d |
| MST11 (stress-induced phosphoprotein 1) | Q60864 | E2 | 1741 | 1.53 | 0.0064 | 113 |
| Stress-induced phosphoprotein 1 | Q99L66 | E2 | 1741 | 1.53 | 0.0064 | 101 |
| γ -Soluble NSF attachment protein (γ -SNAP) | Q9CZW7 | E3 | 337 | -1.52 | 0.0048 | 491 |
| Endoplasmic reticulum protein Erp29 precursor | P57759 | E2 | 778 | -2.08 | 0.0058 | 134 |
| Endoplasmic reticulum protein Erp29 precursor | P57759 | E2 | 582 | -1.72 | 0.0112 | 100 |
| Lipoamide acyltransferase component of branched-chain α -keto acid dehydrogenase complex | P53395 | E2 | 1893 | 1.50 | 0.0126 | 87 |
| β -Alanine oxoglutarate aminotransferase homologue (GABA transaminase) | Q8BZA3 | E2 | 240 | -1.71 | 0.0107 | 74 |
| <i>Mus musculus</i> adult male kidney cDNA; gene name; ethe1, synonym: hsc0 | Q9DCM0 | E2 | 782 | -1.56 | 0.0137 | 71 |
| Probable D-tyrosyl-tRNA deacylase | Q9DD18 | E1 | 251 | -1.71 | 0.0004 | 131 |
| GRB2 adapter protein | Q60631 | E2 | 1213 | -1.57 | 0.0100 | 122 |
| Lamin C and C2 | P11516 | E2 | 1207 | 1.86 | 0.0075 | 203 |
| Lamin A | P48678 | E2 | 1207 | 1.86 | 0.0075 | 203 |
| Paraspeckle protein 1 | Q8R326 | E2 | 1207 | 1.86 | 0.0075 | 196 |
| Myeloid leukemia factor 2 | Q99KX1 | E2 | 1609 | -1.56 | 0.0190 | 83 |
| UPF0082 | Q8K0Z7 | E3 | 178 | 1.58 | 0.0086 | 135 |

^a SWISS-PROT/TrEMBL accession number.

^b Sequential extraction fraction where the protein was identified.

^c Mascot protein identification score is $-10 \times \log(P)$, where P is the probability that the observed match is a random event. Protein scores greater than 57 are significant ($p < 0.05$), as based on the mouse database used here.

^d This spot was independently identified twice as stathmin with a Mascot score near to significance. Tandem mass spectra were manually validated, and the identification was considered correct.

and 2 mM EDTA, pH 7.0. State 4 respiration was measured after adding 40 μ l of malate/glutamate (240/280 mM; assay concentration, 4.8/5.6 mM). Then, 10 μ l of ADP (100 mM; assay concentration, 0.5 mM) were added to measure state 3 respiration. After determining coupled respiration, 1 μ l of carbonyl cyanide *p*-trifluoromethoxyphenylhydrazone (FCCP) (0.1 mM; assay concentration, 0.05 mM) was added to the reaction chamber, and respiration was measured in the absence of a proton gradient. To inhibit complex I activity, a total volume of 3 μ l (2 + 1 μ l) rotenone (0.1 mM; final concentration, 0.15 mM) was added. Then, 10 μ l of succinate (1 M; final concentration, 5 mM) were added, and respiration was measured. Finally, 8 μ l of KCN (0.5 M; assay concentration, 2 mM) were added to inhibit complex IV activity. P301L tau mice and WT mitochondria were measured in parallel pairs using the same conditions (crossover design).

Complex I Activity—Isolated mitochondria were solubilized in *n*-dodecyl β -D-maltoside (20%) (Sigma-Aldrich). NADH:hexaammineruthenium(III)-chloride (HAR) activity was measured at 30 °C in a buffer containing 2 mM Na⁺/MOPS, 50 mM NaCl, and 2 mM KCN, pH 7.2, using 2 mM HAR and 200 μ M NADH as substrates to estimate the complex I content. To determine NADH-ubiquinone oxidoreductase activity, 100 μ M *n*-decylubiquinone (DBQ) and 100 μ M NADH were used as substrates, as described previously (29). Oxidation rates of NADH were recorded with a Shimadzu Multi Spec-1501 diode array spectro-

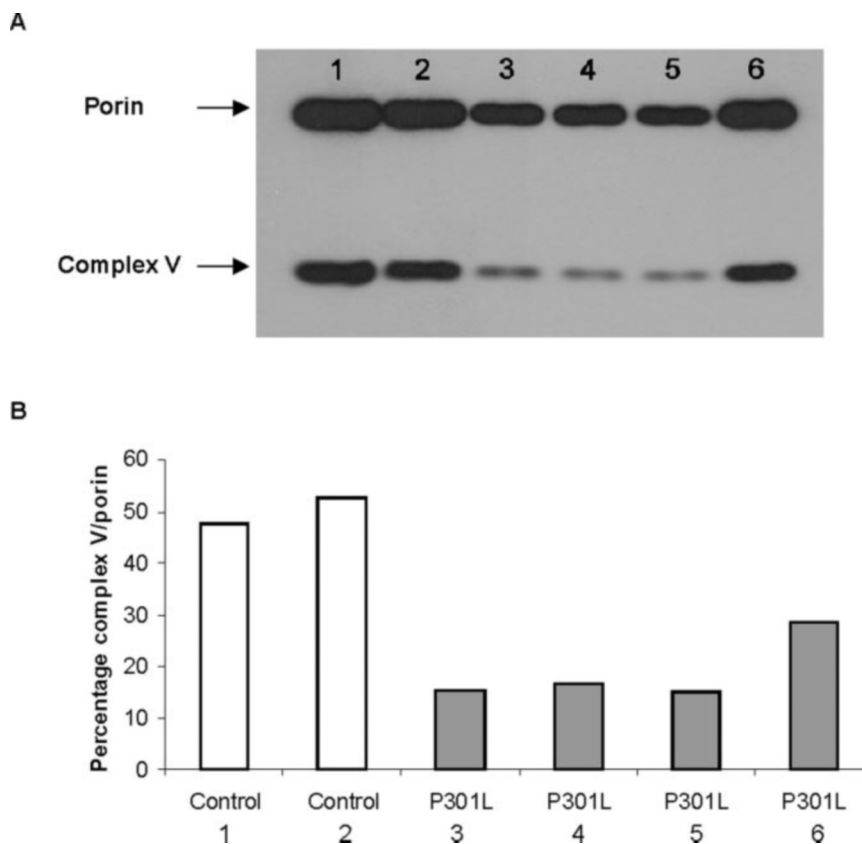
photometer ($\epsilon_{340-400 \text{ nm}} = 6.1 \text{ mM}^{-1} \text{ cm}^{-1}$). Complex I activity was normalized to the complex I content of the mitochondrial preparation and is given as DBQ/HAR ratio.

Complex IV Activity—Cytochrome *c* oxidase activity was determined in intact isolated mitochondria using the Cytochrome *c* Oxidase Assay Kit. The colorimetric assay is based on the observation that a decrease in absorbance at 550 nm of ferrocytochrome *c* is caused by its oxidation to ferricytochrome *c* by cytochrome *c* oxidase. The Cytochrome *c* Oxidase Assay was performed as described previously (30).

Preparation of Brain Hemispheres to Determine Lipid Peroxidation and Antioxidant Enzyme Activities—Mice were anesthetized, and blood was removed by transcardial perfusion with phosphate-buffered saline, pH 7.4. One hemisphere was minced in 1 ml of cold 20 mM Tris-buffered saline with 10 strokes in a Potter homogenizer at 1200 rpm (the other hemisphere was fixed in paraformaldehyde). An aliquot of this homogenate was diluted 1:1 with Tris-buffered saline and centrifuged at 3000 $\times g$ for 10 min at 4 °C, and supernatants were collected and stored at -80 °C for lipid peroxidation assays. The remaining homogenate was centrifuged at 8500 $\times g$ for 10 min at 4 °C, and supernatants were collected and stored at -80 °C until antioxidant enzyme activity determination.

Assay of Lipid Peroxidation Products—The lipid peroxidation product malondialdehyde (MDA) was determined by a photometrical

FIG. 2. Reduced complex V levels in human P301L FTDP-17 brains. *A*, Western blot of human temporal cortex brain homogenates. Complex V (ATP synthase) is recognized as the *bottom band* using an anti-ATP synthase D chain antibody, and the mitochondrial protein marker porin is recognized as the *top band* using an anti-porin antibody. Control brain homogenates were loaded in *lanes 1 and 2*, and P301L FTDP-17 brain homogenates were loaded in *lanes 3–6*. *B*, complex V/porin percentages for control and P301L brains after Western blot band quantification. Sample percentages are represented in the same order as on the Western blot described in *A*.



method using the Lipid Peroxidation Assay Kit (Calbiochem) (31). The colorimetric reaction is a condensation of the aldehyde with 1-methyl-2-phenylindole, yielding a chromophore with an absorption maximum at 586 nm. Basal levels of MDA were assayed after incubation of samples for 30 min at 37 °C, and stimulated MDA levels were determined under the same conditions in the presence of 50 μM FeCl_3 in the sample homogenate.

Cu,Zn-SOD Activity—Cu,Zn-SOD (EC 1.15.1.1) activity was measured with the Superoxide Dismutase Assay Kit (Calbiochem) (32). To remove interfering substances and rule out Mn-SOD activity, Cu,Zn-SOD enzyme activity was assayed after an extraction procedure with chloroform and ethanol according to the supplier's manual. SOD activity was calculated based on the V_s/V_c ratio of the auto-oxidation rates of the chromophore BXT-01050 measured at 37 °C in the presence (V_s) and absence (V_c) of sample. The chromophore was measured in a Genesys 5 photometer (Spectronic Instruments, Rochester, NY) at 525 nm. 1 Cu,Zn-SOD activity unit is defined as the activity that doubles the auto-oxidation background ($V_s/V_c = 2$).

Glutathione Peroxidase Activity—Glutathione peroxidase (cytosolic glutathione peroxidase, EC 1.11.1.9) activity was measured using the Cellular Glutathione Peroxidase Assay Kit (Calbiochem) (33) and *tert*-butylhydroperoxide as substrate. This reaction is based on the enzymatic reduction of hydroperoxide by glutathione peroxidase under consumption of reduced glutathione, which is restored from oxidized glutathione in a coupled enzymatic reaction by glutathione reductase (GR). GR reduces oxidized glutathione to reduced glutathione under consumption of NADPH as reducing equivalents. The decrease in absorbance at 340 nm due to NADPH consumption was measured in a Victor2 multiplate reader using a 355-nm filter with 40 nm bandpass. 1 unit of glutathione peroxidase is defined as the activity that converts 2 μmol reduced glutathione/min at 25 °C.

GR Activity—The GR (EC 1.8.1.7.) activity was determined using the Glutathione Reductase Assay Kit (Calbiochem) (34). The enzymatic activity was assayed photometrically by measuring NADPH consumption during the enzymatic reaction. In the presence of oxidized glutathione and NADPH, GR reduces oxidized glutathione and oxidizes NADPH to yield NADP, resulting in a decrease of absorbance at 340 nm, which was measured in a Victor2 plate reader. 1 unit of GR is defined as the activity that reduces 1 μmol oxidized glutathione (corresponding to 1 μmol NADPH/min at 25 °C).

Statistical Analysis—Data are represented as means \pm S.E. For statistical comparison, Student's *t* test, one-way ANOVA followed by

Tukey's *post hoc* test, or two-way ANOVA followed by Bonferroni *post hoc* tests was used. Only *p* values of <0.05 were considered statistically significant.

RESULTS

Proteomic Analysis of P301L Tau Transgenic Mice—We performed a proteomic study to carry out an unbiased characterization of the consequences of the expression of the human P301L mutant tau in a transgenic mouse model. To favor the visualization of a relatively large proportion of different proteins on two-dimensional gels, the brain proteins were sequentially extracted in three fractions according to their solubility, namely, E1 (soluble proteins), E2 (intermediate soluble proteins), and E3 (less soluble proteins). The proteins of each fraction from six pairs of hemizygous P301L tau and WT control mice were first focused in 17-cm IPG strips depending on their isoelectrical point (pI) and then resolved in the second dimension by their molecular mass on SDS-PAGE gels. Silver staining revealed reproducible two-dimensional protein patterns for each sequentially extracted fraction (Fig. 1). Differences between transgenic and WT mice were highlighted by the Proteomweaver software, which normalizes the overall spot intensities and then performs a comparison of every gel with every other gel. Protein spots that differed by >1.5 -fold and were statistically significant by Student's *t* test ($p < 0.05$) were considered for further investigation. Overall, we found 15 up-regulated and 22 down-regulated protein spots in P301L tau transgenic mice as compared with WT controls, including 4 up- and 4 down-regulated protein spots in fraction E1, 10 up- and 17 down-regulated protein spots in fraction E2, and 1 up- and 1 down-regulated protein spot in the last fraction, E3. After trypsinization, all but three of these differentially regulated protein spots were identified by MALDI-TOF/TOF mass spectrometry (Table I). Several spots contained more than one protein, and some were identified as the same protein.

The majority of the regulated spots identified are related to

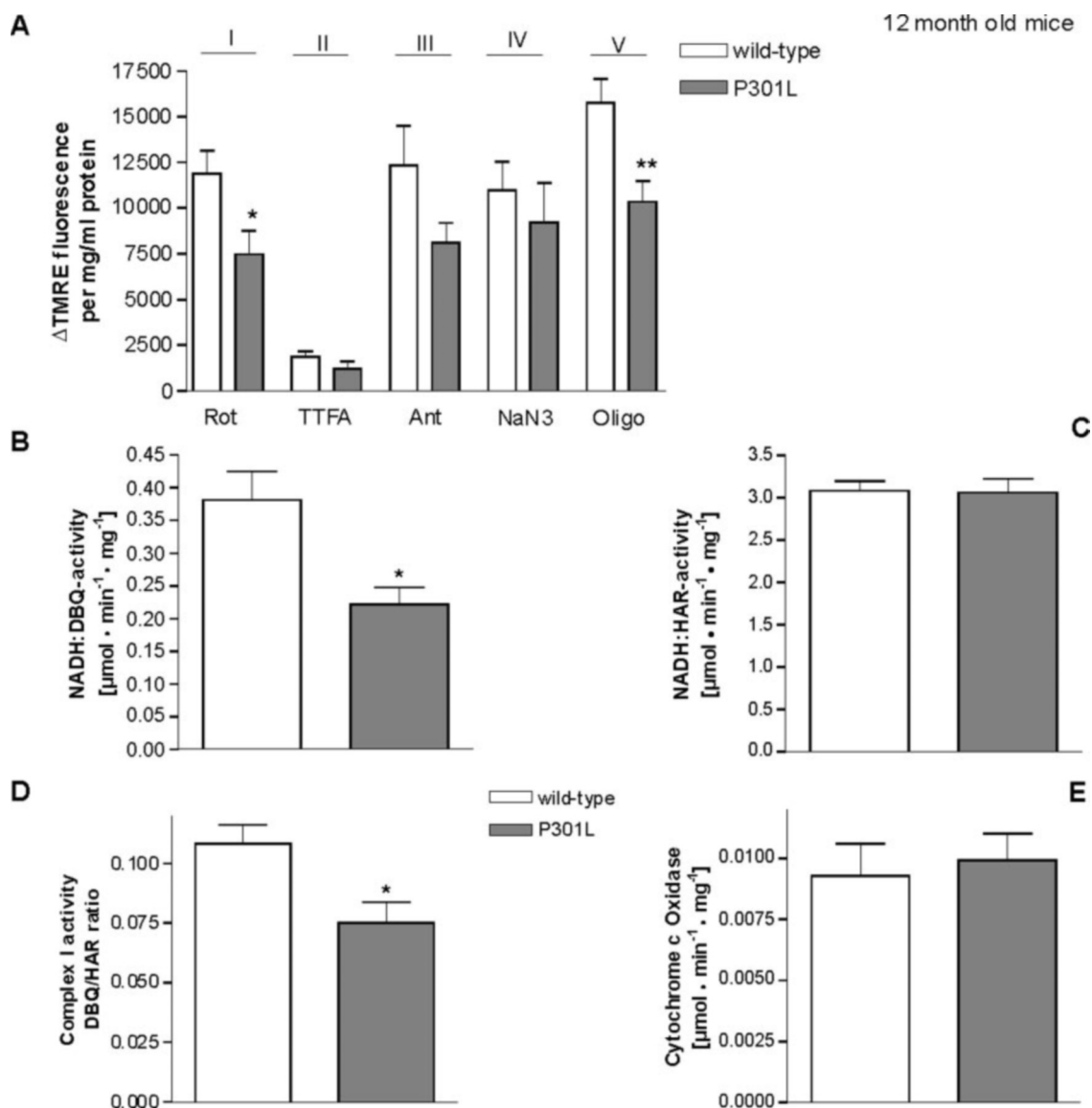


FIG. 3. Impaired depolarization and reduced mitochondrial complex I activity in P301L tau mice. A, use of specific complex inhibitors reveals a significantly reduced depolarization of mitochondria from 12-month-old P301L tau mice after treatment with the complex I inhibitor rotenone (*Rot*) and the complex V inhibitor oligomycin (*Oligo*) (*, $p < 0.05$; **, $p < 0.01$ versus corresponding WT control mice, Student's *t* test). A similar tendency was also found by inhibition of complex II with thenoyltrifluoroacetone, inhibition of complex III with antimycin (*Ant*), and inhibition of complex IV with NaN_3 . Two-way ANOVA reveals a significant effect of the transgene ($p < 0.01$) and individual complexes ($p < 0.001$), with no interaction between the two parameters. B–D, complex I activity in cerebral mitochondria from 12-month-old P301L tau mice and age-matched WT control mice. B, reduced NADH-ubiquinone oxidoreductase (NADH:DBQ) activity in mitochondria of P301L tau mice (*, $p < 0.05$ versus WT control mice, Student's *t* test). C, unaltered NADH:HAR activity. D, complex I activity was normalized to the complex I content of the mitochondrial preparation and is given as DBQ/HAR ratio (*, $p < 0.05$ versus WT control mice, Student's *t* test). E, unaltered complex IV activity. All values represent the means \pm S.E. from $n = 6$ –8 animals/group.

either metabolism and mitochondrial respiration, oxidative stress, or synapse function. In the first category, we identified one spot as the 30-kDa subunit of NADH-ubiquinone oxidoreductase (electron transport chain complex I) and two spots as the ATP synthase D chain (complex V). All three spots were down-regulated as well as the metabolism-related spots, triose-phosphate isomerase, a glycolytic enzyme, and the cytoplasmic malate dehydrogenase involved in the malate-aspartate shuttle providing a metabolic coordination between cytosol and mitochondria. In contrast, a spot identified as inorganic pyrophosphatase was up-regulated. Associated with oxidative stress, spots representing the antioxidant enzymes peroxiredoxin 6, periredoxin 3 (thioredoxin-dependent peroxide reductase), glutathione *S*-transferase (GST) P2 and Mu1, and phospholipid hydroperoxide glutathione peroxidase were all down-regulated. In the last functional category, we found up-regulated spots

related to synaptic function, such as the synaptic vesicle-associated proteins synapsin I, CDCrel-1, and septin 11, the axonal growth-related protein dihydropyrimidinase-related protein (DRP)-2, and another member of the dihydropyrimidinase family, DRP-3. Further differentially regulated spots (Table I) included stathmin, a microtubule-destabilizing protein; MST11, the murine homologue of hop (HSP70/HSP90 organizing protein); and growth factor receptor-bound protein 2 (GRB2), an adapter protein in signaling pathways. Therefore, P301L tau expression results in distinct modifications of the brain proteome, suggesting alterations in the mitochondrial electron transport chain, cellular antioxidant capacities, and synaptic properties.

Human P301L FTDP-17 Brains Show Decreased Complex V Levels—Because the proteomics comparison of the P301L tau and WT control mice revealed a significant decrease of two

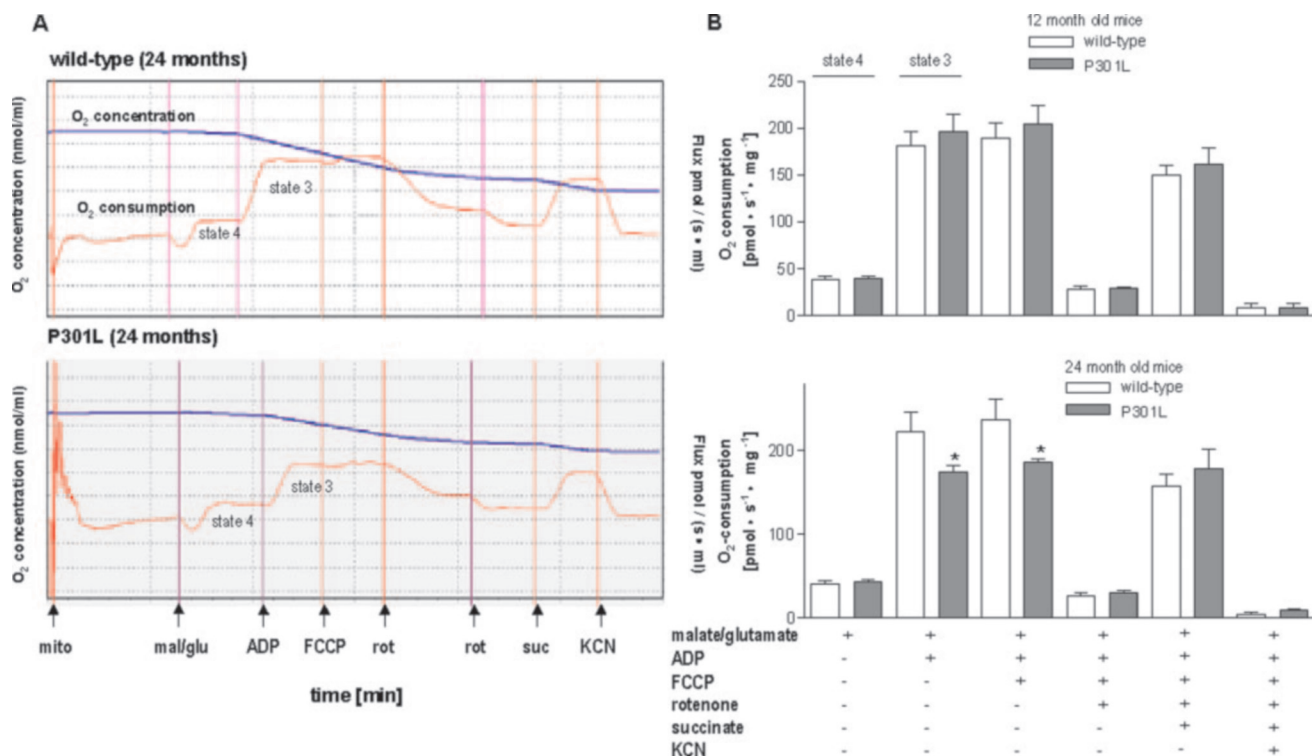


FIG. 4. Oxygen electrode reveals a reduction of O₂ consumption of P301L tau mitochondria during aging. *A*, representative diagrams of measurement of oxygen (O₂) consumption in mitochondria from a 24-month-old WT control (*top panel*) and an age-matched P301L tau mouse (*bottom panel*) demonstrating a decrease in the total O₂ concentration with time. O₂ flux and consumption by mitochondria (*mito*) was measured after addition of different agents (marked by arrows): malate/glutamate (*mal/glu*; state 4), ADP (state 3), FCCP, rotenone (*rot*), succinate (*suc*), and KCN. *B*, O₂ consumption in freshly isolated cerebral mitochondria from 12-month-old mice (*top panel*) and 24-month-old mice (*bottom panel*), respectively. State 4 was measured after adding malate/glutamate. Then, ADP was added to measure state 3 respiration. After determining coupled respiration, FCCP was added, and respiration was measured in the absence of a proton gradient. To inhibit complex I activity, rotenone was added. Then, respiration was measured after the addition of succinate. Finally, complex IV activity and O₂ consumption were inhibited by treatment with KCN. Two-way ANOVA reveals a significant effect of the transgene ($p < 0.05$) on coupled (state 3 and 4) and FCCP-induced uncoupled respiratory rates of mitochondria from 24-month-old P301L tau mice compared with age-matched WT controls by using the specific complex I substrates malate/glutamate. Thus, aged but not 12-month-old P301L tau mice exhibit a significant impairment of complex I-related respiration (*, $p < 0.05$ versus corresponding WT control, Student's *t* test), whereas respiratory rates after addition of the complex II substrate succinate are unchanged. Values represent the means \pm S.E. from $n = 4$ animals/group (measurement of WT control and P301L tau in parallel). All experiments were performed in duplicates.

spots identified as the ATP synthase D chain, we looked at complex V levels in human FTDP-17 patient brains carrying the P301L tau mutation. Four P301L FTDP-17 brain and two control brain homogenates were examined by Western blot (Fig. 2A). We used the mitochondrial protein marker porin to control for variations in mitochondrial amounts. Normalization of complex V levels with porin levels showed a significant decrease in complex V levels in all P301L brain samples compared with control brains (Fig. 2B). Similar control complex V/porin percentages were found in three other control brain samples (data not shown). On average, we measured a 62.3% reduction of complex V levels in P301L FTDP-17 brains compared with control brains. The decreased levels of complex V in human P301L FTDP-17 brains confirm the proteomics observation made in the P301L tau transgenic mice and suggest that the P301L mutant tau pathology potentially causes a specific mitochondrial dysfunction in humans as well as in mice.

P301L Tau Mice Exhibit Mitochondrial Respiratory Defects—We examined the metabolic capacity and function of cerebral mitochondria from P301L tau transgenic mice. Consistent with the down-regulation of subunits of mitochondrial electron transport chain complexes I and V, treatment with specific complex inhibitors showed a general reduction in mitochondrial depolarization of P301L tau brain cells compared with WT and specifically showed a significantly reduced depolarization after inhibition of complexes I and V (Fig. 3A). Using a direct measurement of complex I activity, we observed a

significant reduction of NADH-ubiquinone oxidoreductase (NADH:DBQ) activity in mitochondria of 12-month-old P301L tau mice (Fig. 3B), whereas NADH:HAR activity (Fig. 3C) was not different, indicating that complex I content is similar in P301L tau and WT control mice. Thus, P301L tau mitochondria present a functional defect of complex I activity with a reduction of 30.75% as revealed after normalization of complex I activity with complex I content (Fig. 3D). In contrast, complex IV showed no differences in the cytochrome *c* oxidase activity between WT and P301L tau transgenic mice (Fig. 3E).

In addition, we determined the state 3 and state 4 respiration using substrates for complex I (glutamate/malate) (Fig. 4, A and B). State 3 respiration measures the capacity of mitochondria to metabolize oxygen and the selected substrate in the presence of a limited quantity of ADP, which is a substrate for the ATP synthase (complex V). State 4 respiration measures respiration when all ADP is exhausted, and it is associated with proton leakage across the inner mitochondrial membrane. Therefore, it represents a “basal-coupled” rate of respiration. Whereas state 3 and state 4 respiration remained unchanged with complex I substrates in 12-month-old P301L tau mice (Fig. 4B, *top panel*), a significantly reduced state 3 respiration could be observed in 24-month-old P301L tau mice (Fig. 4, A and B, *bottom panels*), leading to a markedly reduced respiratory control ratio compared with age-matched WT mice (Fig. 5A). The respiratory control ratio provides a measure for the efficiency of coupling of the mitochondrial respiratory chain,

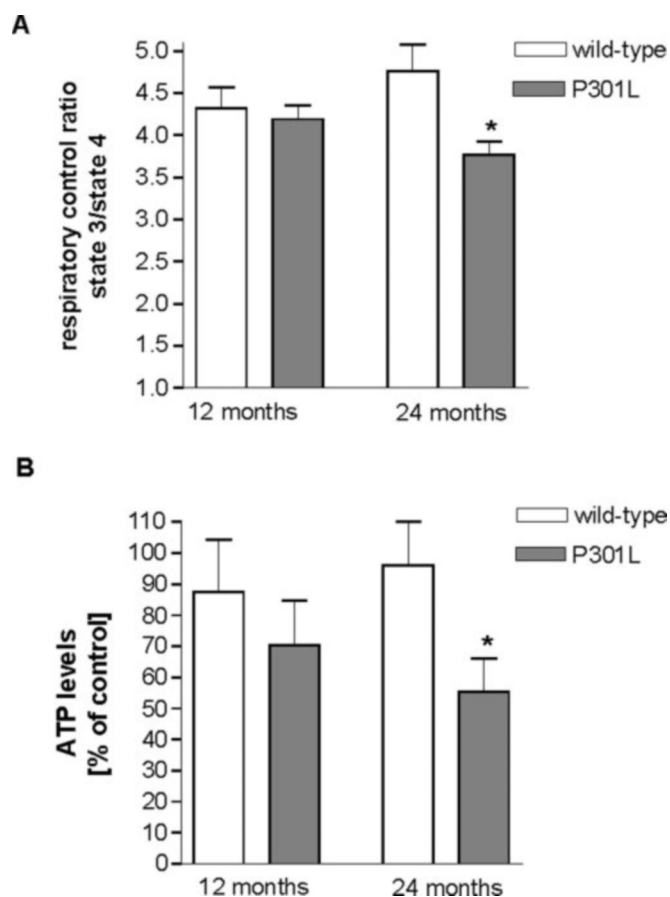


FIG. 5. Reduced respiratory control ratio and impaired ATP synthesis in P301L tau mice with aging. *A*, reduced respiratory control ratio in 24-month-old P301L tau mitochondria (*, $p < 0.05$ versus age-matched WT control mice, Student's *t* test), indicating an impaired efficiency of electron transport in aging. Values represent means \pm S.E. from $n = 4$ animals/group. All experiments were done in duplicates. *B*, in accordance, cerebral ATP levels are significantly reduced in 24-month-old P301L tau mice (*, $p < 0.05$ versus age-matched WT control mice, Student's *t* test). Two-way ANOVA reveals a significant effect of the transgene ($p < 0.05$) on ATP levels. Values represent means \pm S.E. from $n = 6-7$ animals/group.

indicating that the relative efficiency of metabolic coupling of the electron chain complexes is impaired during aging in P301L tau mice. In addition, after uncoupling with FCCP, the respiratory rate in the absence of a proton gradient was significantly diminished in 24-month-old P301L tau mice (Fig. 4*B*, bottom panel), indicating a reduced maximum capacity of the electron transport chain. After complete inhibition of complex I with rotenone, succinate was added as a substrate for complex II. No difference in respiratory rate could be observed between transgenic and WT mice, showing that complex II is not impaired by P301L tau. In accordance with the respiratory control ratio, ATP levels of cerebral cells were unchanged in 12-month-old P301L tau transgenic mice but significantly reduced with aging (Fig. 5*B*). Together, these results suggest that P301L tau mice exhibit an initial defect in mitochondrial function with reduced complex I activity, which, with age, is translated into a mitochondrial respiration deficiency with diminished ATP synthesis corresponding to reduced complex V activity.

Mitochondrial Dysfunction Is Not Coupled to Alterations in the Number of Mitochondria in P301L Tau Mice—Evaluation of the number of mitochondria in cerebral brain cells revealed no difference between P301L tau and WT mice either in the cerebrum (Fig. 6*A*) or in the cerebellum (data not shown). In addition, co-immunostaining of mitochondria and microtubules and subsequent counting of the mitochondria in proximal and

distal parts of neurites in the CA1 region of the hippocampus also showed no variation between P301L tau and WT mice (Fig. 6*B*). These data suggest that mitochondrial dysfunction is not associated with reduced mitochondrial numbers or significant changes in transport of mitochondria along neurites.

Increased Tau Pathology Causes Higher Oxidative Stress, Modified Lipid Peroxidation Levels, and Up-regulation of Antioxidant Enzyme Activities in P301L Tau Mice—In P301L tau mice, these mitochondrial defects are associated with increased ROS formation because both staining with DHE for detection of superoxide anions and staining with $H_2DCF-DA$ for detection of cytosolic peroxides were increased (Fig. 7, *A* and *B*). Increased ROS levels could be detected already in 12-month-old P301L tau mice but were more pronounced and statistically significant in 24-month-old mice, correlating with the age-specific increase in tau pathology. As a measure of free radical damage to critical cellular components, levels of MDA as lipid peroxidation end product were determined. Despite increased ROS levels, basal levels of MDA were decreased in 24-month-old hemizygous P301L tau mice and more pronounced in homozygous mice, indicating that ROS levels are met by adequate antioxidant defenses in these mice (Fig. 7*C*). However, upon stimulation with ferric iron, increased MDA levels were formed in P301L tau mice (Fig. 7*D*). This effect was already observed in 12-month-old mice but was more pronounced and statistically significant in 24-month-old homozygous mice. Furthermore, basal and stimulated MDA levels remained unchanged in the cerebellum of 24-month-old hemi- and homozygous P301L tau and WT mice (data not shown). Because P301L tau is expressed at very low levels in the cerebellum (7), we can conclude that modifications in lipid peroxidation are specifically caused by the presence of the P301L tau protein. Hence, the presence of mutant tau impairs antioxidant defense under conditions of increased oxidative stress.

As a direct measure of antioxidant defense, activities of antioxidant enzymes were determined. Although no significant changes were observed in 12-month-old mice, 24-month-old homozygous P301L tau mice displayed increased activities of Cu,Zn-SOD and GR (Fig. 8, top and bottom), whereas the activity of glutathione peroxidase was not significantly increased (Fig. 8, middle). The increased enzyme activities may provide protection against ROS damage under basal conditions, but they are obviously not sufficient to eliminate lipid peroxidation damage caused by the *in vitro* stimulation of brain homogenates with ferric iron. It is important to note that modified lipid peroxidation levels and increased antioxidant enzyme activities are dependent on the levels of P301L tau pathology because these changes were only detected as significant in old homozygous P301L tau mice.

$A\beta$ Insult Causes Increased Membrane Potential Reduction in P301L Tau Mitochondria—Extracellular $A\beta$ treatment of PC12 cells has been shown to lead to a significant decrease in mitochondrial membrane potential (35). To investigate whether brain cells from P301L tau mice are more susceptible to $A\beta$, we measured the mitochondrial membrane potential of isolated cortical brain cells with and without $A\beta$ treatment. Interestingly, the basal mitochondrial membrane potential was still conserved in cerebral cells from P301L tau mice. However, secondary insult with $A\beta_{1-42}$ resulted in a higher reduction in membrane potential in P301L tau mitochondria than in WT mitochondria (Fig. 9*A*). Importantly, this effect is brain region-specific and therefore probably dependent on the presence of P301L tau because cells from cerebellum with very low P301L tau expression levels were not vulnerable to this damage (Fig. 9*B*). These data suggest a synergistic action of $A\beta$ and tau pathology on mitochondrial function.

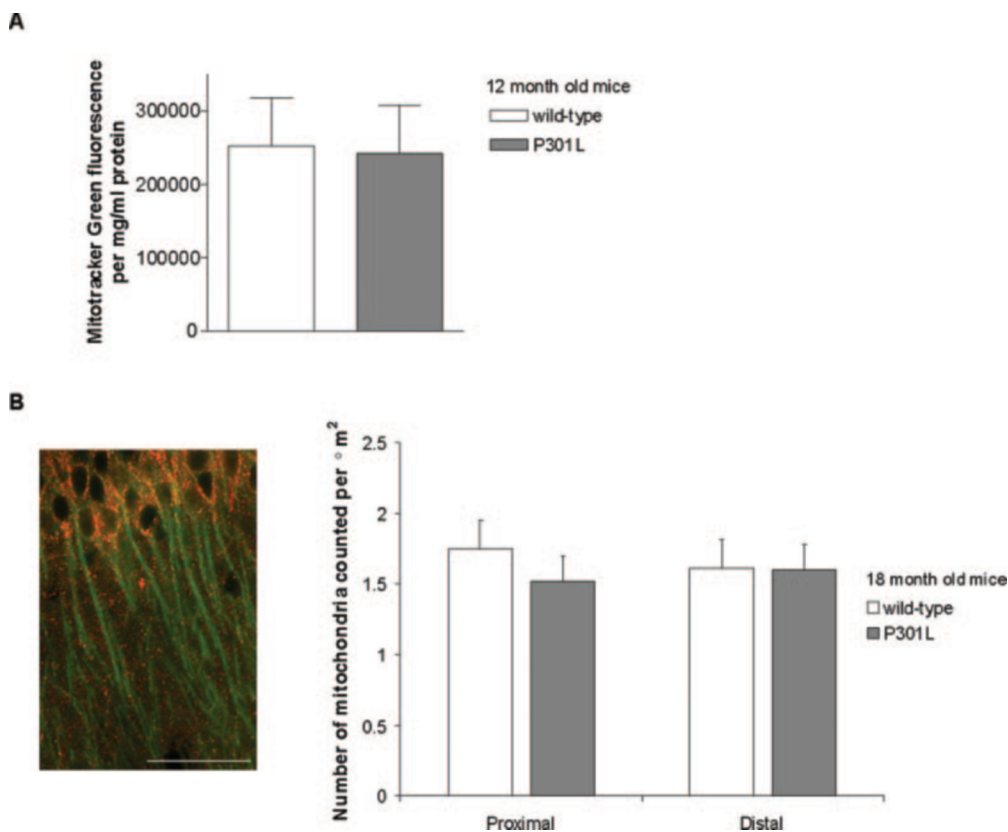


FIG. 6. Unchanged number of mitochondria. *A*, measurement of the number of mitochondria using the cell-permeable mitochondrion-selective dye Mitotracker Green reveals no differences between P301L tau and WT mice in cerebrum. Values represent the means \pm S.E. from $n = 8$ animals/group. *B*, immunostaining of mitochondria and microtubules in CA1 hippocampal brain sections with anti-porin (Cy3; red) and anti-tubulin antibodies (Cy2; green) again reveals no statistical difference in mitochondrial neuritic numbers in proximity or distal to the cell body between 18-month-old P301L tau and WT mice. Values represent the means \pm S.D. from $n = 4$ animals/group, in which mitochondria were counted in four different neurites per animal. Scale bar, 50 μm .

DISCUSSION

The P301L mutation of tau is one in a set of mutations implicated in FTDP-17 (36). This mutation reduces the ability of tau to interact with microtubules and promotes the assembly of tau into filaments *in vitro*. In our P301L tau transgenic mice, tau filaments start to accumulate at about 6 months of age, preceded by distinct hyperphosphorylation of tau (7, 20). Furthermore, the tau pathology causes specific behavioral deficits in the mice related to the amygdala, an area with prominent NFT formation (37).

Proteomics is becoming more and more widely used to study brain changes under physiological and pathological conditions such as in AD (38, 39). Considering the complexity of brain tissue, we adapted a sequential extraction method to separate the brain proteins according to solubility before proteomic analysis (40). This approach, followed by functional analysis of the P301L tau mice, suggests that tau accumulation, in the absence of massive NFT formation, induces a mitochondrial dysfunction. The down-regulation of nuclear encoded subunits of electron transport chain complexes I and V was accompanied by a reduced depolarization of mitochondria from 12-month-old P301L tau mice after treatment with the complex I inhibitor rotenone and the complex V inhibitor oligomycin. We could also demonstrate a direct decrease in complex I activity. At this age, the other mitochondrial respiratory chain complexes seemed to be able to compensate because the respiratory control ratio and mitochondrial membrane potential remained unchanged. However, following the increase of tau pathology with aging, this compensation is no longer sufficient, and mitochondria from 24-month-old P301L tau mice exhibited an impaired efficiency of coupling between the mitochondrial respiratory chain com-

plexes, diminished capacity in electron transport, and a significant reduction in ATP levels. In particular, the reduction in state 3 respiration reflects a reduced capacity of mitochondria to metabolize oxygen and the complex I substrate in the presence of a limited quantity of ADP. Thus, there is also a clear complex I deficiency in the mitochondrial respiration at 24 months of age.

Our results correlate with previous studies on AD, suggesting partial mitochondrial uncoupling (41), modifications of mitochondrial encoded complex I subunit mRNA (42, 43), and reduction in protein levels of the 24- and 75-kDa subunits of complex I (11) as well as diminished ATP synthase (complex V) levels (10). As demonstrated in primates, complex I activity has been shown to be reduced with aging, which could potentially intensify complex I activity defects in the P301L tau mice (44). Furthermore, we could show a clear-cut reduction in levels of complex V in human P301L FTDP-17 brains as compared with control human brains. This important finding confirming the decrease in complex V identified twice in our proteomics analysis of the P301L tau mouse argues in favor of a potential mitochondrial dysfunction in human FTDP-17 patients. This result also emphasizes the relevance of our P301L tau mouse as a model of the human tau pathology.

Our proteomic analysis also revealed modifications in levels of triosephosphate isomerase, cytoplasmic malate dehydrogenase, and inorganic pyrophosphatase, implying a broader metabolic disorder possibly encompassing the glycolysis cycle. The glycolytic enzyme triosephosphate isomerase can bind to microtubules (45), and higher levels of nitrated triosephosphate isomerase have been found in AD brains (46). Consistent with an overall metabolic failure, several

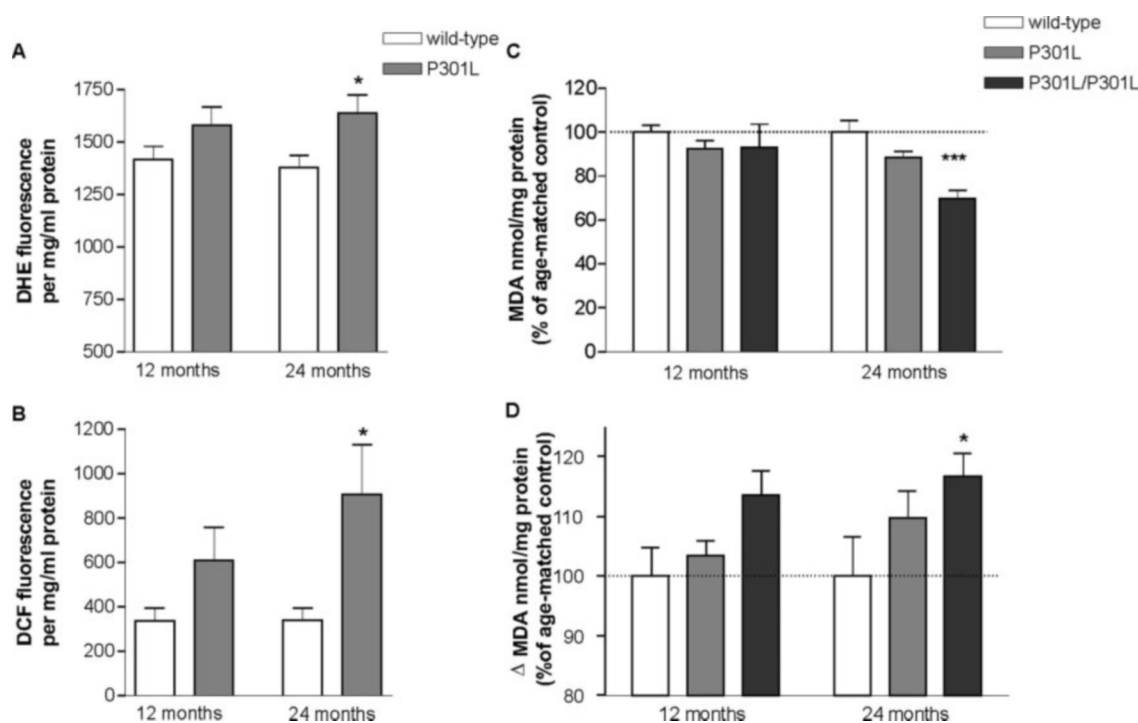


FIG. 7. Increased ROS production. A, increases in superoxide anion radicals determined by DHE oxidation. Fluorescence (in arbitrary units) normalized for protein content in brain cells from hemizygous P301L tau mice was measured after incubation of samples with DHE for 15 min. Two-way ANOVA: $p < 0.01$, effect of transgene; age and interaction were not significant. Bonferroni *post hoc* test: *, $p < 0.05$, WT versus hemizygous P301L tau mice. B, increases in cytosolic H_2O_2 determined by H_2DCF oxidation. Fluorescence in brain cells from hemizygous P301L tau mice was measured after incubation of samples with H_2DCF -DA for 15 min. Two-way ANOVA: $p < 0.01$, effect of transgene; age and interaction were not significant. Bonferroni *post hoc* test: *, $p < 0.05$, WT versus hemizygous P301L tau mice. C, reduced lipid peroxidation in P301L tau brains under basal conditions determined by MDA levels (nmol/mg protein). Two-way ANOVA: $p < 0.01$, effect of transgene; $p < 0.05$, age group; $p < 0.05$, interaction. Bonferroni *post hoc* test: ***, $p < 0.001$, WT versus homozygous P301L tau mice (P301L/P301L). D, increased lipid peroxidation under stimulated conditions in 24-month-old homozygous P301L tau mice. Formation of MDA (nmol/mg protein) in brain homogenates after a 30-min incubation with $FeCl_3$ is increased in samples from P301L tau mice. Two-way ANOVA: $p < 0.05$, effect of transgene; age and interaction were not significant. Bonferroni *post hoc* test: *, $p < 0.05$, controls versus homozygous P301L tau mice. All values represent means \pm S.E. from $n = 6$ –9 animals/group (except for 12-month-old homozygous animals, $n = 3$).

reports using positron emission tomography revealed reduced glucose metabolism in AD and frontotemporal dementia brains (12, 13, 47–49). Notably, high levels of phosphorylated tau have been linked to glucose hypometabolism in mild cognitively impaired patients (50).

Together, this evidence supports a role of tau pathology in mitochondrial and metabolic dysfunction. However, it remains unclear how tau accumulation mediates these changes. Overexpression of WT tau in cell culture caused impairment of plus end-directed transport, resulting in a reduction of mitochondria levels in the neurites (51). Although we cannot exclude the possibility of this occurring in the P301L tau mice, the number of mitochondria in neurites counted in proximity or distally to the cell body did not vary significantly compared with WT numbers. Furthermore, the total amount of mitochondria remained unchanged as measured in brain cells of transgenic compared with control mice. This suggests that either P301L tau induces a different pathological mechanism than overexpressed WT tau or that tau action on mitochondria transport in cell culture cannot be extrapolated over to the mouse model. Consistent with our findings, similar numbers of mitochondria were reported in NFT-bearing and non-NFT-bearing cells in AD (52). Alternatively, tau accumulation could have direct repercussions on the mitochondria because the accumulation of increasingly insoluble ATP synthase α -chain together with NFTs has been shown in AD brains, whereas detergent soluble levels were reduced (53). Overall, it is important to note that the mitochondrial pathology in the P301L tau mice observed in this study is unlikely to be a direct consequence of tau hyperphosphorylation. Indeed, the transgene levels of expression in

these mice are relatively low (7), and depletion of ATP solely due to tau hyperphosphorylation would be improbable.

We furthermore demonstrate that accumulation of P301L tau causes significant modifications in the oxidative state of the brain. ROS measurements revealed increased levels of cytosolic H_2O_2 and superoxide anion radicals in 2-year-old P301L tau mice. These increased ROS levels may be a direct consequence of reduced complex I activity in P301L tau mice because inhibition of complex I can lead to increased superoxide formation (54). The increased activity of Cu,Zn-SOD measured in P301L tau mice should ameliorate the accumulation of superoxide but also gives rise to H_2O_2 , which is then insufficiently processed by glutathione peroxidase, leading to accumulation of peroxides. Accordingly, the relative increase in H_2O_2 in P301L tau mice was much more pronounced than the increase in superoxide radicals. Somewhat unexpectedly, along with increased tau pathology, we observed decreased levels of the lipid peroxidation product MDA as a marker for ROS damage to cellular membranes in old homozygous P301L tau mice, despite increased levels of ROS. One potential explanation for this discrepancy could be that the cells affected by lipid peroxidation are removed by apoptosis, although we could not detect major differences in levels of apoptotic cells detected by terminal deoxynucleotidyl transferase-mediated nick end labeling staining (data not shown). Because several steps lead from ROS accumulation to lipid peroxidation damage, another possibility would be that the up-regulation of antioxidant activities of Cu,Zn-SOD and GR in P301L tau mice may intercept ROS before they can critically damage membranes. As previously reported, rising Cu,Zn-SOD and GR activities in aged mouse

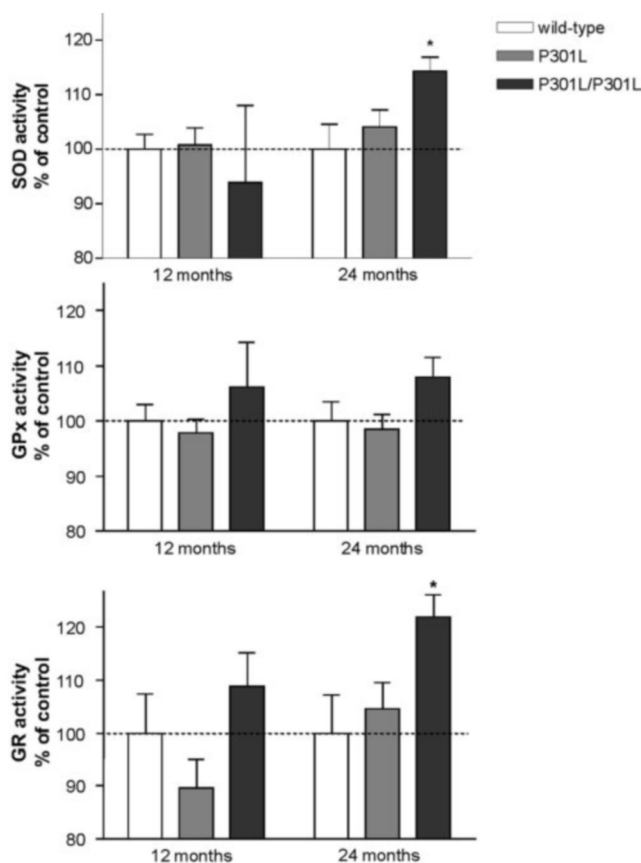


FIG. 8. Altered levels in detoxifying enzymes. *Top*, increased Cu,Zn-SOD activity in 24-month-old homozygous P301L tau mice. Two-way ANOVA: effect of transgene was not significant; $p < 0.05$, age group; $p < 0.05$, interaction. Bonferroni *post hoc* test: *, $p < 0.05$, controls *versus* homozygous P301L tau mice. *Middle*, glutathione peroxidase activity. Two-way ANOVA: $p < 0.05$, effect of transgene; age group and interaction were not significant. *Bottom*, increased GR activity in 24-month-old homozygous P301L tau mice. Two-way ANOVA: $p < 0.05$, effect of transgene; age group and interaction were not significant. Bonferroni *post hoc* test: *, $p < 0.05$, controls *versus* homozygous P301L tau mice. Values represent means \pm S.E. from $n = 6-9$ animals/group (except for 12-month-old homozygous animals, $n = 3$).

brains can protect against lipid peroxidation (55). Furthermore, SOD can prevent lipid peroxidation both *in vitro* and *in vivo* (56–60). Similarly, increased GR activity in P301L tau mice may protect against accumulation of MDA by increasing levels of the antioxidant reduced glutathione. In several experimental models, increased levels of reduced glutathione were associated with lower levels of lipid peroxidation products and vice versa (61, 62). Upon *in vitro* stimulation, however, higher levels of MDA were formed in homozygous P301L tau brain homogenates. Obviously, the increased activities of Cu,Zn-SOD and GR were not sufficiently protective under these conditions. This may be explained by a relative lack in glutathione peroxidase activity because the accumulation of H_2O_2 observed in brains from P301L tau mice combined with the exogenously added ferric iron can lead to increased formation of hydroxyl radicals via Haber-Weiss and Fenton reactions. Reports on lipid peroxidation in brains from patients with tauopathies are inconsistent. Although increased levels of the lipid peroxidation product 4-hydroxynonenal were found in patients with progressive supranuclear palsy (63), and tau was co-localized with MDA immunoreactivity in AD patients (64), another study reported increased lipid peroxidation products specifically in AD patients, but not in patients with frontotemporal dementia (65). Therefore, tau pathology may not be associated

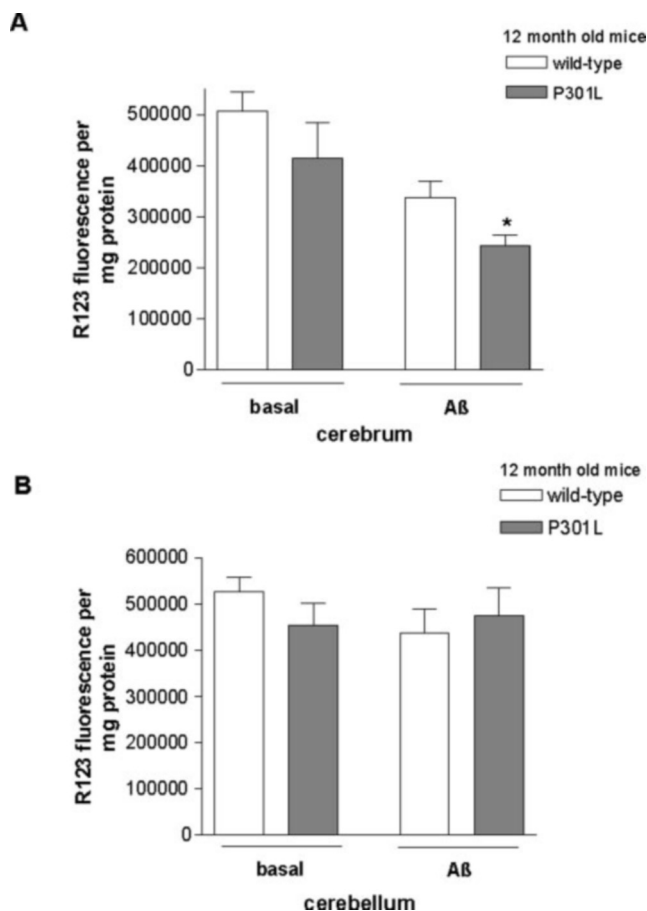


FIG. 9. Brain region-specific decrease of membrane potential after secondary insult with 50 nM A β . Aged, aggregated preparations of A β_{1-42} were given to brain cells as secondary insult. An increased reduction of $\Delta\psi_m$ was observed with the addition of A β to cerebral cells (A) (*, $p < 0.05$ *versus* WT control mice, Student's *t* test), but not with cerebellar cells (B) from 12-month-old P301L tau mice. Two-way ANOVA reveals a significant effect of the transgene ($p < 0.05$) on changes of mitochondrial membrane potential in cerebral cells. Values represent the means \pm S.E. from $n = 6-7$ animals/group.

inevitably with lipid peroxidation processes in human brain tissue, consistent with our observations in P301L tau mice. Most studies have reported an up-regulation of antioxidant enzyme activities in AD (66). These changes were most pronounced in brain regions that are severely affected by AD pathology (66–68).

Our proteomic analysis also suggests changes in cellular antioxidant mechanisms as shown by variations in spots representing the antioxidant enzymes periredoxin 3, peroxiredoxin 6, GST P2 and Mu1, and phospholipid hydroperoxide glutathione peroxidase. Peroxiredoxin reduces peroxides including H_2O_2 , GST catalyzes the conjugation of reduced glutathione to a large number of molecules, and phospholipid hydroperoxide glutathione peroxidase directly reduces peroxidized phospholipids in membranes (69). Although all these protein spots were down-regulated in the P301L tau mouse, this does not necessarily reflect enzyme activities. Besides, under oxidative conditions, these antioxidant enzymes are prone to oxidative modifications represented by a set of distinct spots on two-dimensional gels as suggested for peroxiredoxin, which undergoes overoxidation. Interestingly, AD brains show decreased GST activity (70) and GST Omega1 mRNA levels in AD (43), and single nucleotide polymorphisms in GST Omega1 are associated with age at onset in AD (43).

Hence, both our functional and proteomic data indicate a complex regulation and potential malfunction of the cellular

antioxidant defense mechanisms in response to increased ROS levels in this mouse model. Because mitochondrial dysfunction appears prior to oxidative stress, this suggests that it is probably the initiating factor. However, we can speculate that both mitochondrial dysfunction and oxidative stress act in synergy, creating a vicious cycle. Indeed, increases in ROS and antioxidant enzyme dysfunction could affect the integrity of the mitochondria and, in particular, the electron transport chain (35). Furthermore, glutathionylation of complex I in oxidative conditions leads to increased superoxide production (71). Another possible consequence of higher oxidative stress levels could be an acceleration of tau pathology (72, 73). Moreover, tau can be readily oxidized by H₂O₂ to form disulfide-linked species that manifest reduced propensity to promote microtubule assembly (74). Oxidized tau then becomes a substrate of the thioredoxin reductase and glutathione/glutaredoxin reductase systems (74, 75). Thereby, we can speculate that the accumulation of oxidized P301L tau might overload these antioxidant regenerating systems, causing further oxidative stress.

Results from our proteomic study further suggest a potential synaptic dysfunction because we found an up-regulation of a series of synapse-related proteins. The identified DRP-2 is known to promote axonal growth by interaction with the tubulin heterodimer and has also been shown to induce neurite formation (76, 77). Synapsin I is thought to regulate the reserve pool of synaptic vesicles (78). The septin member CDCrel-1 is found mainly in inhibitory presynaptic terminals and inhibits exocytosis (79, 80). Interestingly, both DRP-2 and septin associate with NFTs in AD (81, 82). Therefore, in response to tau pathology, the transgenic mouse neurons may be attempting a compensatory mechanism by increasing synaptic vesicle control proteins and potentially aberrant synaptic sprouting. Indeed, although advanced stages of AD are associated with synaptic loss, an initial increase in synaptic protein levels in AD brains was observed that was correlated with the appearance of the tau pathology but not with A β plaques (83). On the contrary, a decrease of synaptic proteins occurred only after the appearance of the full spectrum of tau and A β pathology. Although it is uncertain exactly how tau mechanistically affects synapses, we can postulate that the mutant tau acts either by modifying microtubule stability and axonal transport or by inhibiting energy production through complex I in the synapses. Indeed, a reduction in the activity of complex I by only 25% has been shown to impair energy metabolism in synaptic mitochondria (84), whereas at least a 72% reduction in complex I activity is needed before energy metabolism is impaired in non-synaptic mitochondria (85). In this study, our mitochondrial isolation does not include synaptic mitochondria. It would be interesting to measure complex I activity and mitochondrial respiration in a pure synaptosomal mitochondrial preparation.

In addition to the three major categories (metabolism-related proteins, antioxidant enzymes, and synaptic proteins), we could identify, by proteomics, several other proteins modified by the presence of the P301L tau and potentially linked to AD pathology. The up-regulated MST11 mediates assembly of HSP70/HSP90 (86). A proteomic study has shown modifications in various chaperone levels in AD brain (87). In addition, levels of HSP α B-crystallin, HSP27, and HSP60 were found to be increased in tauopathies with glial pathology (88). Decreased in the P301L tau mouse brain proteome pattern, GRB2 is an adapter protein that is involved in the activation of the mitogen-activated protein kinase signaling pathway. Interestingly, AD brains show higher amounts of GRB2 than control brains (89, 90). Levels of the microtubule-destabilizing protein stathmin have been found to be negatively correlated with NFT

numbers in AD neocortex (91) and were also down-regulated in the P301L tau mice.

Finally, our data from the proteomic and functional study of the P301L tau transgenic mouse should help to better distinguish between the respective pathological actions of A β and tau protein. Numerous studies indicate that A β also causes oxidative stress and mitochondrial malfunction (35, 92–94). In particular, A β has been shown to generate free radicals *in vitro* (95) and reduces mitochondrial respiration through inhibition of cytochrome *c* oxidase activity (35, 96). We show here that A β causes increased reduction of mitochondrial membrane potential in P301L tau mouse cerebrum compared with wild-type cerebrum. Importantly, this is not observed in the cerebellum of P301L tau mice, a brain area with very low levels of transgenic tau. This could partially explain why injection of fibrillar A β peptide into the hippocampus of P301L tau mice accelerated NFT formation in the amygdala, in line with the amyloid cascade hypothesis (20). Therefore, both tau and A β accumulation probably act in synergy on oxidative stress and mitochondrial dysfunction.

In conclusion, our study increases understanding of the pathological consequences of tau alone, suggesting that not only A β but also tau accumulation acts on the metabolism of the brain and the oxidative conditions in AD. This implies that it will be important to address the treatment and/or removal of both A β and tau pathology to efficiently treat AD patients.

Acknowledgments—We thank Dr. Robert Layfield for helpful suggestions; Dr. Peter Gehrig for excellent assistance with mass spectrometry; the Functional Genomics Center Zürich for providing access to the MALDI-TOF/TOF apparatus, GelPix robot, and Proteomweaver software; Ilka Siebels for excellent technical assistance; and James Opoku for animal care.

REFERENCES

- Lee, V. M., Goedert, M., and Trojanowski, J. Q. (2001) *Annu. Rev. Neurosci.* **24**, 1121–1159
- Gotz, J., Streffer, J. R., David, D., Schild, A., Hoerndli, F., Pennanen, L., Kurosinski, P., and Chen, F. (2004) *Mol. Psychiatry* **9**, 664–683
- Poorkaj, P., Bird, T. D., Wijsman, E., Nemens, E., Garruto, R. M., Anderson, L., Andreadis, A., Wiederholt, W. C., Raskind, M., and Schellenberg, G. D. (1998) *Ann. Neurol.* **43**, 815–825
- Hutton, M., Lendon, C. L., Rizzu, P., Baker, M., Froelich, S., Houlden, H., Pickering-Brown, S., Chakraverty, S., Isaacs, A., Grover, A., Hackett, J., Adamson, J., Lincoln, S., Dickson, D., Davies, P., Petersen, R. C., Stevens, M., de Graaff, E., Wauters, E., van Baren, J., Hillebrand, M., Joosse, M., Kwon, J. M., Nowotny, P., Che, L. K., Norton, J., Morris, J. C., Reed, L. A., Trojanowski, J., Basun, H., Lannfelt, L., Neystat, M., Fahn, S., Dark, F., Tannenber, T., Dodd, P. R., Hayward, N., Kwok, J. B., Schofield, P. R., Andreadis, A., Snowden, J., Craufurd, D., Neary, D., Owen, F., Oostra, B. A., Hardy, J., Goate, A., van Swieten, J., Mann, D., Lynch, T., and Heutink, P. (1998) *Nature* **393**, 702–705
- Spillantini, M. G., Murrell, J. R., Goedert, M., Farlow, M. R., Klug, A., and Ghetti, B. (1998) *Proc. Natl. Acad. Sci. U. S. A.* **95**, 7737–7741
- Lewis, J., McGowan, E., Rockwood, J., Melrose, H., Nacharaju, P., Van Slegtenhorst, M., Gwinn-Hardy, K., Murphy, P. M., Baker, M., Yu, X., Duff, K., Hardy, J., Corral, A., Lin, W. L., Yen, S. H., Dickson, D. W., Davies, P., and Hutton, M. (2000) *Nat. Genet.* **25**, 402–405
- Gotz, J., Chen, F., Barmettler, R., and Nitsch, R. M. (2001) *J. Biol. Chem.* **276**, 529–534
- Mattson, M. P., Pedersen, W. A., Duan, W., Culmsee, C., and Camandola, S. (1999) *Ann. N. Y. Acad. Sci.* **893**, 154–175
- Mutisya, E. M., Bowling, A. C., and Beal, M. F. (1994) *J. Neurochem.* **63**, 2179–2184
- Schagger, H., and Ohm, T. G. (1995) *Eur. J. Biochem.* **227**, 916–921
- Kim, S. H., Vlkolinsky, R., Cairns, N., Fountoulakis, M., and Lubeck, G. (2001) *Life Sci.* **68**, 2741–2750
- Jagust, W. J., Seab, J. P., Huesman, R. H., Valk, P. E., Mathis, C. A., Reed, B. R., Coxson, P. G., and Budge, T. F. (1991) *J. Cereb. Blood Flow Metab.* **11**, 323–330
- Santens, P., De Bleecker, J., Goethals, P., Strijckmans, K., Lemahieu, I., Slegers, G., Dierckx, R., and De Reuck, J. (2001) *Eur. Neurol.* **45**, 19–27
- Shoffner, J. M., Brown, M. D., Torroni, A., Lott, M. T., Cabell, M. F., Mirra, S. S., Beal, M. F., Yang, C. C., Gearing, M., Salvo, R., Watts, R. L., Juncos, J. L., Hansen, L. A., Crain, B. J., Fayad, M., Reckord, C. L., and Wallace, D. C. (1993) *Genomics* **17**, 171–184
- Corral-Debrinski, M., Horton, T., Lott, M. T., Shoffner, J. M., McKee, A. C., Beal, M. F., Graham, B. H., and Wallace, D. C. (1994) *Genomics* **23**, 471–476
- Coskun, P. E., Beal, M. F., and Wallace, D. C. (2004) *Proc. Natl. Acad. Sci. U. S. A.* **101**, 10726–10731
- Hajimohammadreza, I., and Brammer, M. (1990) *Neurosci. Lett.* **112**, 333–337

18. Sayre, L. M., Zelasko, D. A., Harris, P. L., Perry, G., Salomon, R. G., and Smith, M. A. (1997) *J. Neurochem.* **68**, 2092–2097
19. Marcus, D. L., Thomas, C., Rodriguez, C., Simberkoff, K., Tsai, J. S., Strafaci, J. A., and Freedman, M. L. (1998) *Exp. Neurol.* **150**, 40–44
20. Gotz, J., Chen, F., van Dorpe, J., and Nitsch, R. M. (2001) *Science* **293**, 1491–1495
21. Rabilloud, T., Carpentier, G., and Tarroux, P. (1988) *Electrophoresis* **9**, 288–291
22. Stoll, L., Schubert, T., and Muller, W. E. (1992) *Neurobiol. Aging* **13**, 39–44
23. Lowry, O. H., Rosebrough, N. J., Farr, A. L., and Randall, R. J. (1951) *J. Biol. Chem.* **193**, 265–275
24. Krohn, A. J., Wahlbrink, T., and Prehn, J. H. (1999) *J. Neurosci.* **19**, 7394–7404
25. Collins, T. J., Berridge, M. J., Lipp, P., and Bootman, M. D. (2002) *EMBO J.* **21**, 1616–1627
26. Crouch, S. P., Kozlowski, R., Slater, K. J., and Fletcher, J. (1993) *J. Immunol. Methods* **160**, 81–88
27. Kenney, A. M., and Kocsis, J. D. (1998) *J. Neurosci.* **18**, 1318–1328
28. Budd, S. L., Castilho, R. F., and Nicholls, D. G. (1997) *FEBS Lett.* **415**, 21–24
29. Djafarzadeh, R., Kerschner, S., Zwicker, K., Radermacher, M., Lindahl, M., Schagger, H., and Brandt, U. (2000) *Biochim. Biophys. Acta* **1459**, 230–238
30. Rasmussen, U. F., and Rasmussen, H. N. (2000) *Mol. Cell. Biochem.* **208**, 37–44
31. Esterbauer, H., and Cheeseman, K. H. (1990) *Methods Enzymol.* **186**, 407–421
32. Nebot, C., Moutet, M., Huet, P., Xu, J. Z., Yadan, J. C., and Chaudiere, J. (1993) *Anal. Biochem.* **214**, 442–451
33. Paglia, D. E., and Valentine, W. N. (1967) *J. Lab. Clin. Med.* **70**, 158–169
34. Mizuno, Y., and Ohta, K. (1986) *J. Neurochem.* **46**, 1344–1352
35. Keil, U., Bonert, A., Marques, C. A., Scherping, I., Weyermann, J., Strosznajder, J. B., Muller-Spahn, F., Haass, C., Czech, C., Pradier, L., Muller, W. E., and Eckert, A. (2004) *J. Biol. Chem.* **279**, 50310–50320
36. Spillantini, M. G., Van Swieten, J. C., and Goedert, M. (2000) *Neurogenetics* **2**, 193–205
37. Pennanen, L., Welzl, H., D'Adamo, P., Nitsch, R. M., and Gotz, J. (2004) *Neurobiol. Dis.* **15**, 500–509
38. Schonberger, S. J., Edgar, P. F., Kydd, R., Faull, R. L., and Cooper, G. J. (2001) *Proteomics* **1**, 1519–1528
39. Butterfield, D. A., Boyd-Kimball, D., and Castegna, A. (2003) *J. Neurochem.* **86**, 1313–1327
40. Molloy, M. P., Herbert, B. R., Walsh, B. J., Tyler, M. I., Traini, M., Sanchez, J. C., Hochstrasser, D. F., Williams, K. L., and Gooley, A. A. (1998) *Electrophoresis* **19**, 837–844
41. Sims, N. R., Finegan, J. M., Blass, J. P., Bowen, D. M., and Neary, D. (1987) *Brain Res.* **436**, 30–38
42. Aksenov, M. Y., Tucker, H. M., Nair, P., Aksenova, M. V., Butterfield, D. A., Estus, S., and Markesbery, W. R. (1999) *Neurochem. Res.* **24**, 767–774
43. Li, Y. J., Oliveira, S. A., Xu, P., Martin, E. R., Stenger, J. E., Scherzer, C. R., Hauser, M. A., Scott, W. K., Small, G. W., Nance, M. A., Watts, R. L., Hubble, J. P., Koller, W. C., Pahwa, R., Stern, M. B., Hiner, B. C., Jankovic, J., Goetz, C. G., Mastaglia, F., Middleton, L. T., Roses, A. D., Saunders, A. M., Schmechel, D. E., Gullans, S. R., Haines, J. L., Gilbert, J. R., Vance, J. M., Pericak-Vance, M. A., Hulette, C., and Welsh-Bohmer, K. A. (2003) *Hum. Mol. Genet.* **12**, 3259–3267
44. Bowling, A. C., Mutisya, E. M., Walker, L. C., Price, D. L., Cork, L. C., and Beal, M. F. (1993) *J. Neurochem.* **60**, 1964–1967
45. Orosz, F., Wagner, G., Liliom, K., Kovacs, J., Baroti, K., Horanyi, M., Farkas, T., Hollan, S., and Ovadi, J. (2000) *Proc. Natl. Acad. Sci. U. S. A.* **97**, 1026–1031
46. Castegna, A., Thongboonkerd, V., Klein, J. B., Lynn, B., Markesbery, W. R., and Butterfield, D. A. (2003) *J. Neurochem.* **85**, 1394–1401
47. Mielke, R., Schroder, R., Fink, G. R., Kessler, J., Herholz, K., and Heiss, W. D. (1996) *Acta Neuropathol.* **91**, 174–179
48. Diehl, J., Grimmer, T., Drzezga, A., Riemenschneider, M., Forstl, H., and Kurz, A. (2004) *Neurobiol. Aging* **25**, 1051–1056
49. Grimmer, T., Diehl, J., Drzezga, A., Forstl, H., and Kurz, A. (2004) *Dement. Geriatr. Cogn. Disord.* **18**, 32–36
50. Fellgiebel, A., Siessmeier, T., Scheurich, A., Winterer, G., Bartenstein, P., Schmidt, L. G., and Muller, M. J. (2004) *Biol. Psychiatry* **56**, 279–283
51. Ebnet, A., Godemann, R., Stamer, K., Illenberger, S., Trinczek, B., and Mandelkow, E. (1998) *J. Cell Biol.* **143**, 777–794
52. Sumpter, P. Q., Mann, D. M., Davies, C. A., Yates, P. O., Snowden, J. S., and Neary, D. (1986) *Neuropathol. Appl. Neurobiol.* **12**, 305–319
53. Sergeant, N., Watzek, A., Galvan-Valencia, M., Ghestem, A., David, J. P., Lemoine, J., Sautiere, P., Mazat, J., Mazat, J. P., Michalski, J. C., Velours, J., Mena-Lopez, R., and Delacourte, A. (2003) *Neuroscience* **117**, 293–303
54. Turrens, J. F., and Boveris, A. (1980) *Biochem. J.* **191**, 421–427
55. Schuessel, K., Schaefer, S., Bayer, T. A., Czech, C., Pradier, L., Muller-Spahn, F., Muller, W. E., and Eckert, A. (2005) *Neurobiol. Dis.* **18**, 89–99
56. Tien, M., Svingen, B. A., and Aust, S. D. (1981) *Fed. Proc.* **40**, 179–182
57. Gutteridge, J. M., Beard, A. P., and Quinlan, G. J. (1983) *Biochem. Biophys. Res. Commun.* **117**, 901–907
58. Gutteridge, J. M. (1984) *FEBS Lett.* **172**, 245–249
59. Bonnes-Taourel, D., Guerin, M. C., Torrelles, J., Ceballos-Picot, I., and de Paulet, A. C. (1993) *J. Lipid Mediat.* **8**, 111–120
60. Liu, R., Liu, I. Y., Bi, X., Thompson, R. F., Doctrow, S. R., Malfroy, B., and Baudry, M. (2003) *Proc. Natl. Acad. Sci. U. S. A.* **100**, 8526–8531
61. Younes, M., and Siegers, C. P. (1980) *Res. Commun. Chem. Pathol. Pharmacol.* **27**, 119–128
62. Comporti, M. (1987) *Chem. Phys. Lipids* **45**, 143–169
63. Odetti, P., Garibaldi, S., Norese, R., Angelini, G., Marinelli, L., Valentini, S., Menini, S., Traverso, N., Zaccaro, D., Siedlak, S., Perry, G., Smith, M. A., and Tabaton, M. (2000) *J. Neuropathol. Exp. Neurol.* **59**, 393–397
64. Dei, R., Takeda, A., Niwa, H., Li, M., Nakagomi, Y., Watanabe, M., Inagaki, T., Washimi, Y., Yasuda, Y., Horie, K., Miyata, T., and Sobue, G. (2002) *Acta Neuropathol.* **104**, 113–122
65. Yao, Y., Zhukareva, V., Sung, S., Clark, C. M., Rokach, J., Lee, V. M., Trojanowski, J. Q., and Pratico, D. (2003) *Neurology* **61**, 475–478
66. Lovell, M. A., Ehmman, W. D., Butler, S. M., and Markesbery, W. R. (1995) *Neurology* **45**, 1594–1601
67. Karelson, E., Bogdanovic, N., Garlind, A., Winblad, B., Zilmer, K., Kullisaar, T., Vihalemm, T., Kairane, C., and Zilmer, M. (2001) *Neurochem. Res.* **26**, 353–361
68. Schuessel, K., Leutner, S., Cairns, N. J., Muller, W. E., and Eckert, A. (2004) *J. Neural Transm.* **111**, 1167–1182
69. Ursini, F., Maiorino, M., and Gregolin, C. (1985) *Biochim. Biophys. Acta* **839**, 62–70
70. Lovell, M. A., Xie, C., and Markesbery, W. R. (1998) *Neurology* **51**, 1562–1566
71. Taylor, E. R., Hurrell, F., Shannon, R. J., Lin, T. K., Hirst, J., and Murphy, M. P. (2003) *J. Biol. Chem.* **278**, 19603–19610
72. Perez, M., Cuadros, R., Smith, M. A., Perry, G., and Avila, J. (2000) *FEBS Lett.* **486**, 270–274
73. Hartzler, A. W., Zhu, X., Siedlak, S. L., Castellani, R. J., Avila, J., Perry, G., and Smith, M. A. (2002) *Neurobiol. Aging* **23**, 855–859
74. Landino, L. M., Skreslet, T. E., and Alston, J. A. (2004) *J. Biol. Chem.* **279**, 35101–35105
75. Landino, L. M., Robinson, S. H., Skreslet, T. E., and Cabral, D. M. (2004) *Biochem. Biophys. Res. Commun.* **323**, 112–117
76. Inagaki, N., Chihara, K., Arimura, N., Menager, C., Kawano, Y., Matsuo, N., Nishimura, T., Amano, M., and Kaibuchi, K. (2001) *Nat. Neurosci.* **4**, 781–782
77. Fukata, Y., Itoh, T. J., Kimura, T., Menager, C., Nishimura, T., Shiromizu, T., Watanabe, H., Inagaki, N., Iwamatsu, A., Hotani, H., and Kaibuchi, K. (2002) *Nat. Cell Biol.* **4**, 583–591
78. Gitler, D., Takagishi, Y., Feng, J., Ren, Y., Rodriguez, R. M., Wetsel, W. C., Greengard, P., and Augustine, G. J. (2004) *J. Neurosci.* **24**, 11368–11380
79. Beites, C. L., Xie, H., Bowser, R., and Trimble, W. S. (1999) *Nat. Neurosci.* **2**, 434–439
80. Kinoshita, A., Noda, M., and Kinoshita, M. (2000) *J. Comp. Neurol.* **428**, 223–239
81. Kinoshita, A., Kinoshita, M., Akiyama, H., Tomimoto, H., Akiguchi, I., Kumar, S., Noda, M., and Kimura, J. (1998) *Am. J. Pathol.* **153**, 1551–1560
82. Yoshida, H., Watanabe, A., and Ihara, Y. (1998) *J. Biol. Chem.* **273**, 9761–9768
83. Mukaetova-Ladinska, E. B., Garcia-Siera, F., Hurt, J., Gertz, H. J., Xuereb, J. H., Hills, R., Brayne, C., Huppert, F. A., Paykel, E. S., McGee, M., Jakes, R., Honer, W. G., Harrington, C. R., and Wischik, C. M. (2000) *Am. J. Pathol.* **157**, 623–636
84. Davey, G. P., Peuchen, S., and Clark, J. B. (1998) *J. Biol. Chem.* **273**, 12753–12757
85. Davey, G. P., and Clark, J. B. (1996) *J. Neurochem.* **66**, 1617–1624
86. Scheufler, C., Brinker, A., Bourenkov, G., Pegoraro, S., Moroder, L., Bartunik, H., Hartl, F. U., and Moarefi, I. (2000) *Cell* **101**, 199–210
87. Yoo, B. C., Kim, S. H., Cairns, N., Fountoulakis, M., and Lubec, G. (2001) *Biochem. Biophys. Res. Commun.* **280**, 249–258
88. Dabir, D. V., Trojanowski, J. Q., Richter-Landsberg, C., Lee, V. M., and Forman, M. S. (2004) *Am. J. Pathol.* **164**, 155–166
89. McShea, A., Zelasko, D. A., Gerst, J. L., and Smith, M. A. (1999) *Brain Res.* **815**, 237–242
90. Russo, C., Dolcini, V., Salis, S., Venezia, V., Violani, E., Carlo, P., Zambrano, N., Russo, T., and Schettini, G. (2002) *Ann. N. Y. Acad. Sci.* **973**, 323–333
91. Jin, L. W., Masliah, E., Iimoto, D., Deteresa, R., Mallory, M., Sundsmo, M., Mori, N., Sobel, A., and Saitoh, T. (1996) *Neurobiol. Aging* **17**, 331–341
92. Keller, J. N., Pang, Z., Geddes, J. W., Begley, J. G., Germeyer, A., Waeg, G., and Mattson, M. P. (1997) *J. Neurochem.* **69**, 273–284
93. Blanchard, V., Moussaoui, S., Czech, C., Touchet, N., Bonici, B., Planche, M., Canton, T., Jedidi, I., Gohin, M., Wirths, O., Bayer, T. A., Langui, D., Duyckaerts, C., Tremp, G., and Pradier, L. (2003) *Exp. Neurol.* **184**, 247–263
94. Anandatheerthavarada, H. K., Biswas, G., Robin, M. A., and Avadhani, N. G. (2003) *J. Cell Biol.* **161**, 41–54
95. Hensley, K., Carney, J. M., Mattson, M. P., Aksenova, M., Harris, M., Wu, J. F., Floyd, R. A., and Butterfield, D. A. (1994) *Proc. Natl. Acad. Sci. U. S. A.* **91**, 3270–3274
96. Casley, C. S., Canevari, L., Land, J. M., Clark, J. B., and Sharpe, M. A. (2002) *J. Neurochem.* **80**, 91–100